ELSEVIER

Contents lists available at ScienceDirect

# **Materials Today Communications**

journal homepage: www.elsevier.com/locate/mtcomm





# Experimental, and numerical investigation of the electrical resistivity of repaired carbon fiber plates

Nawres J. Al-Ramahi a,b,c,\* , Patrik Fernberg , Greger Nilsson , Roberts Joffe

- <sup>a</sup> Division of Materials Science, Luleå University of Technology, Luleå SE-971 87, Sweden
- <sup>b</sup> Institute of Civil and Mechanical Engineering, Riga Technical University, Riga, Latvia
- <sup>c</sup> Institute of Technology / Baghdad, Middle Technical University, Baghdad, Iraq
- <sup>d</sup> Blade Solutions Inspection & Repair, Öjebyn 943 33, Sweden

#### ARTICLE INFO

Keywords:
Carbon fiber composite
Composite repair
Electrical resistivity
Electrical heating
Finite element method

#### ABSTRACT

This study examines the electrical and thermal performance of carbon fiber prepreg composite laminates for deicing and anti-icing applications, relevant to wind turbine blades and aircraft wings. Both undamaged and damaged plates with various lay-ups, co-cured on a glass fiber composite sandwich, were analyzed. Various electrode attachment techniques were evaluated, with embedded stainless steel strips proving the most effective for uniform current distribution. Electrical resistance was measured by applying voltage and normalizing results to the effective conductive area. The resistance decreased with increasing temperature, demonstrating semiconductor behavior. Fiber orientation also significantly affected electrical resistance and temperature rise, favouring electrical current flow along the fiber directions. Different repair methods for damaged laminates were considered, revealing that repairing multiple layers in one step yields better results than a multi-step approach. A numerical analysis by means of the finite element method using ANSYS software was carried out to simulate the electrical and thermal performance. The difference between simulations and experiments was consistently within 5 % accuracy, confirming the model's reliability. In all, the findings provide valuable insights towards optimized electrical performance of carbon fiber composites in aerospace and energy applications.

#### 1. Introduction

The comprehensive and adaptable applications of carbon fiber-reinforced plastics (CFRPs) arise from the excellent combination of their specific mechanical properties and the notable electrical performance of carbon fibers (CFs). These characteristics have enabled a growing range of multifunctional uses, including de-icing aircraft components, preventing ice accumulation on wind turbine blades, and manufacturing heated CFRP molds. Advances in non-destructive evaluation techniques, particularly electrical measurements, have further enhanced the ability to detect and assess damage in CFRPs [1]. Significant research has also explored the Joule effect as a progressive, non-destructive method for identifying interlaminar flaws in CFRP materials [2]. In addition, CFRPs have been effectively applied in antennas [3], aircraft [4], automobiles [5], concrete reinforcement [6], and transducers [7].

Electrical resistance in a CFRP plate represents its opposition to current flow, primarily governed by the conductive CFs, while the polymer matrix limits conductivity. Electrical conductivity, the inverse of resistivity, quantifies how easily electrons move through the composite. For multilayer CFRPs, accurate measurement of conductivity is critical to determine their suitability in such applications.

Laminated CFRPs with continuous fibers are typically classified as unidirectional (UD) or multidirectional. The conductivity of UD CFRPs and UD dry carbon fiber preforms has been widely studied, with influencing factors including fiber conductivity, orientation [7–10], volume fraction [11], temperature [12], and ply thickness [13]. Recently, attention has grown toward using electrical resistance variations to evaluate long-term structural performance in health monitoring systems [14–19]. The conductivity of CFs enables the formation of sensing networks within the composite. Resistance changes can result from fiber breakage [1,20], delamination [21–24], deformation [16,25,26], and temperature changes [27]. The interaction between conductive fibers in a dielectric matrix, monitored under varying temperature or humidity, has also been extensively examined [28–30].

Electrical resistance measurement is an effective means of tracking

<sup>\*</sup> Corresponding author at: Division of Materials Science, Luleå University of Technology, Luleå SE-971 87, Sweden. *E-mail address*: nawres.al-ramahi@associated.ltu.se (N.J. Al-Ramahi).

damage under diverse load conditions, including tension [26], compression [31], flexure [32], interlaminar shear [33], fatigue [34], and low-velocity impact [35]. Resistance changes can be correlated directly with damage progression [36]. Resistivity along the fiber axis can indicate fiber breakage, while through-thickness resistivity can show delamination [37].

Enhancing CFRP conductivity can be achieved by adding conductive fibers, forming randomly distributed conductive channels within an insulating matrix. Depending on their distribution, CFRPs may display conductive or insulating behaviour [38,39]. Their layered structure results in electrical anisotropy, with conductivity being highest along the fiber direction and significantly lower perpendicular to it [40]. Compared to metals, UD CFRPs exhibit approximately three orders of magnitude lower conductivity along the fiber direction and up to four orders of magnitude lower conductivity in the transverse direction [40].

In idealized models, ignoring the contact between fibers due to overlapping, electricity is assumed to flow along CFs, with the polymer acting as an insulator. Perfectly straight, isolated fibers would yield extremely high insulation perpendicular to the fibers. In practice, however, transverse conductivity exists due to fiber waviness and occasional contact between adjacent fibers [41]. A similar pattern occurs out-of-plane, though here the resin layer between plies limits conduction. For the prepreg used in this study, out-of-plane conductivity is markedly lower than 90° in-plane conductivity. Since conduction in both directions depends on fiber contacts, the total composite resistance reflects resistance across all fibers [42]. Higher fiber volume fractions increase the likelihood of contact, but resin-rich regions between plies can reduce through-thickness conductivity [43].

Damage in CFRP plates has been addressed in multiple studies [44–50], with repair methods categorized by: (a) damage severity, (b) location, and (c) aerodynamic/flush requirements. Repairs fall into three groups: 1- Erosion repair and protection – coatings, tapes, or shields; 2- Non-structural repairs – minor cracks or small delaminations treated by filling, sealing, or resin injection; 3- Structural repairs – significant damage requiring plug/patch or scarf repairs.

Heslehurst [44,45] identified four repair zones for blades: Zone 1-Leading edge – flush repairs for aerodynamic efficiency; Zone 2- Near the tip, behind the leading edge – aeroelastic semi-structural repairs; Zone 3- Midsection between tip and root, including trailing edge – flush repairs; Zone 4- Near or at the root – semi-structural or structural repairs.

Bonded repairs are widely used to maintain integrity. For wind turbine blades, flush repairs are preferred for aerodynamic performance, involving the removal of the damaged section and bonding of a precisely shaped patch with tapered or stepped edges [46]. Wet lay-up methods are common, with unidirectional or biaxial uncured prepregs, matching the original material, often used for patches [47–49]. External patches can restore 50–100 % of original strength for skins up to ~16 plies thick [46], though they may introduce eccentric load paths, bending forces, adhesive stress, and reduced buckling stability. Bonded configurations include scarf, stepped scarf (both maintaining a smooth aerodynamic surface), and overlap repairs [50]. For maximum strength, scarf joints are generally preferred [48], particularly for delamination in spar caps, in-service impact damage, and manufacturing defects like fiber waviness or resin voids.

There are also several recent reviews [51–54] that provide important insights into the advancement of anti-icing and de-icing technologies. Cui et.al. [51] presents a comprehensive overview of integrated aircraft systems, highlighting progress in electrothermal methods, functional—structural integration, and emerging multifunctional approaches tailored to lightweight composite structures. Zhang et.al. [52] examines next-generation materials that combine passive and active strategies, such as superhydrophobic, photothermal, electrothermal, and self-healing designs (to deliver durable), energy-efficient, and all-weather performance. In the field of wind energy, the review by Li et. al [53] surveys current ice protection systems for wind turbines and

identifies electro-impulse and pneumatic methods, adapted from aerospace, as particularly promising for improving both efficiency and mitigation effectiveness. Finally, the review by Zhao et.al [54] addresses the rapid development of biomimetic coatings, where micro-nano surface structuring and physicochemical strategies enable super-hydrophobicity, lubrication, and anti-freezing properties. Together, these studies emphasize the importance of multifunctional and synergistic approaches while outlining the challenges and future directions for high-performance ice-phobic technologies.

Notwithstanding the extensive research conducted, certain phases remain insufficiently studied regarding repair efficiency and the effects of fiber orientation. These can be specified as follows:

- Examining the impact of monoclinic materials (off-axis layers of composite laminates) and mixed fiber orientations on electrical resistance and heat generation.
- Investigating whether repair patches can restore electrical pathways in CFRP and how various bonding techniques influence conductivity and structural health monitoring capabilities.
- Conducting experimental and numerical studies to better understand the influence of ply stacking sequences and interlaminar conductivity pathways on overall electrical behavior.

Accordingly, this study will address these gaps by systematically investigating these aspects. Through a combination of experimental analysis and numerical modeling, we will evaluate the influence of monoclinic materials and mixed fiber orientations on electrical resistance and heat generation. Additionally, we will assess the effectiveness of different repair patch strategies in restoring electrical pathways, examining how various bonding techniques impact both conductivity and structural health monitoring. Finally, we will explore the role of ply stacking sequences and interlaminar conductivity pathways in shaping the overall electrical behavior of CFRP, providing new insights that can contribute to the advancement of composite material applications in aerospace, automotive, and other high-performance engineering fields. The investigation is limited to short-term performance, with long-term durability aspects such as cyclic loading, environmental exposure, and adhesion fatigue excluded from the current analysis.

## 1.1. Sample manufacturing and measurement setup

The fast-curing carbon fiber prepreg (T700S/#2300 product by TORAYCA) was used to fabricate composite laminates with dimensions of  $200 \times 200 \, \text{mm}^2$ . A sandwich panel made of glass fiber composites and polymer foam core (supplied by PODCOMP AB, Piteå, Sweden) with dimensions of  $230 \times 230 \times 30 \, \text{mm}^3$  was used as a support material for the carbon fiber layers (to simulate the structure of the turbine blade). The prepreg was cured on top of the sandwich panel (the number of layers and the thickness of each carbon fiber composite laminate as described later in Section 4.1). The whole assembly (carbon fiber layer, glass fiber panel, and stainless-steel electrodes) was placed in a hot press (Phi Pasadena Hydraulics, inc) at  $130^{\circ}\text{C}$ , 3 bar for 30 min, ensuring proper curing for the matrix. This manufacturing setup was used for all the samples in this study.

Before executing experiments measuring electrical conductivity and heat generation within the carbon plate, electrodes (the types of connections for electrodes are described/discussed later in the text) were connected to a DC power supply using M5 steel bolts and nuts to ensure a stable connection between the wires and electrodes. To prevent heat reflection from surrounding surfaces from interfering with the thermal camera, a protective shield (enclosure) made of glass fiber sandwich panels was used, as shown in Fig. 1. For consistent comparison across different plates, a constant voltage of 2 V was applied in all tests. A FLIR A6000 thermal camera (with IR resolution:  $640\times512$  pixels and measurement accuracy:  $\pm$  2% of reading), along with ResearchIR software, was employed to monitor the temperature increase and distribution



Fig. 1. Experimental setup for measuring temperature distribution in a laminate subjected to electrical current using an infrared (IR) camera.

within the plate throughout the experiment. It is worth mentioning that, to assess variability, each test was repeated three times. The reported results represent the average values, with differences between repeated measurements remaining within 3%. For cases where the results exhibited larger scatter, all data points are presented in full.

Various methods were employed to supply current to the plate, but most of them resulted in hotspots at the connection points. Hotspots arise at the electrical connection points between the electrode and the carbon fiber plate, driven by factors such as contact resistance, surface roughness, and non-uniform current distribution across the interface. The methods tested include: 1) wires attached through holes drilled in the composite plate by steel bolts and nuts (M5), the contact is provided through the thickness and surfaces of the carbon composite and the bolt head with washer positioned between the net and the composite, as shown in Fig. 2-a; and 2) a  $180\times17~x~2.5~mm^3$  copper bars were clamped on a sanded (to remove the resin layer and expose carbon fibers) carbon plate using three M5 steel bolts and nuts, as shown in Fig. 2-b

Unfortunately, neither of these methods worked, as they resulted in a poor connection between the electrode and the carbon plate, creating hotspot areas at the connection points, as shown in Figs. 3-a and 3-b. To

improve the connection, a conductive epoxy adhesive was applied between the copper electrode and the carbon composite (adhesive was cured for one hour at room temperature) as shown in Fig. 2-c. While this technique enabled a strong current flow between the electrodes, as shown in Fig. 3-c (demonstrating significant improvement over previous methods), it also resulted in high costs (labor and materials). This is acceptable for the test on a laboratory scale but it is not going to be feasible approach for real-life applications. Thus, this method was not employed in this study. To overcome these issues, a new technique was introduced that outperformed the earlier methods. This involved embedding a steel strip (as an electrode with dimensions  $300 \times 15 \text{ x}$   $1.5 \text{ mm}^3$ ) between pairs of prepreg carbon fiber layers, creating full contact along the plate's length, as shown in Fig. 2-d. This approach eliminated hotspots and ensured a uniform distribution of current across the plate, as shown in Fig. 3-d.

The distance between the metal strips defines the effective width of the plate (160 mm). Assembly was cured the same way as described earlier. Two materials were tested as an electrode: aluminum and stainless steel. The aluminum strip developed an oxidation layer during the curing of pre-preg, resulting in poor contact with the carbon fibers. While the stainless steel electrodes demonstrated superior contact with the carbon fibers, and this method was chosen for all tests in the study.

#### 1.2. Determining plate resistance through voltage-current measurements

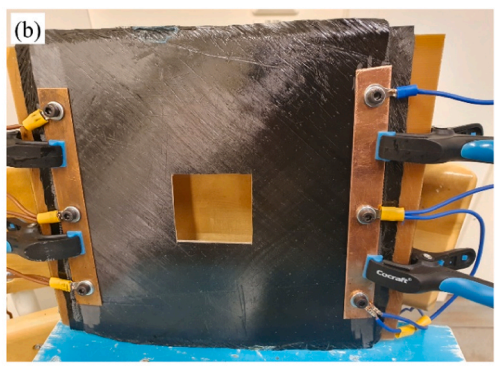
To determine the electrical resistance (R = V/I) of the plate, various voltages V (from 1 V to 18 V) were systematically applied to the plate while measuring the corresponding currents I according to the electrical circuit in Fig. 4.

#### 1.3. Theoretical estimation of plate resistance based on fiber orientation

This part of the study focuses on evaluating the impact of fiber orientation on the equivalent resistance of plates. Resistivity is a fundamental property of materials. Therefore, when manufacturing plates with different fiber orientations using the same type of carbon







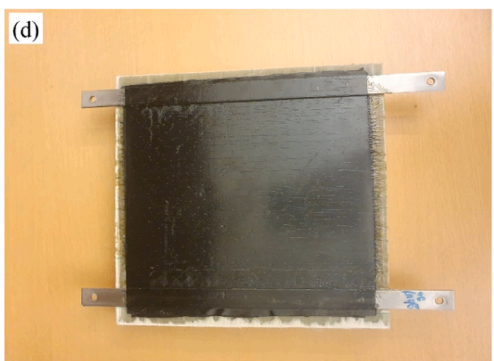


Fig. 2. Sample with four connection methods: a) connecting wires to the plate by bolts and nuts, b) using copper bars between the bolts and the carbon plate, c) using a conductive epoxy adhesive between the copper bar and carbon plate, d) inserting a steel strip in between the carbon layers.

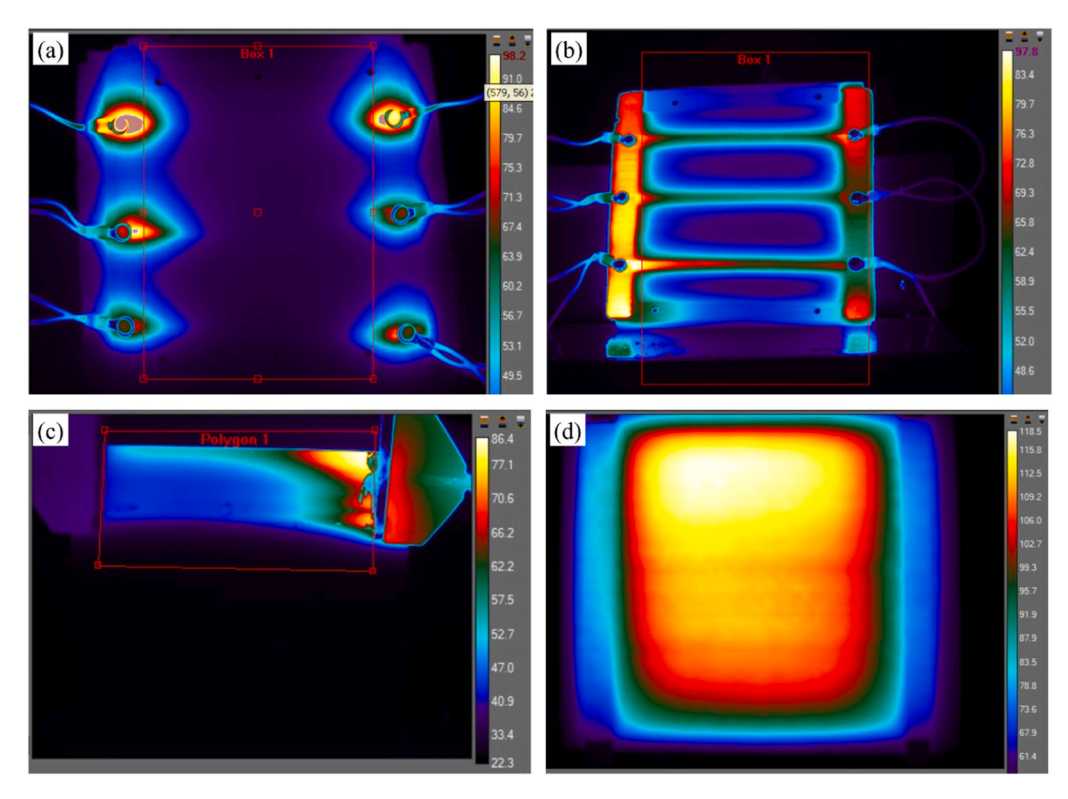
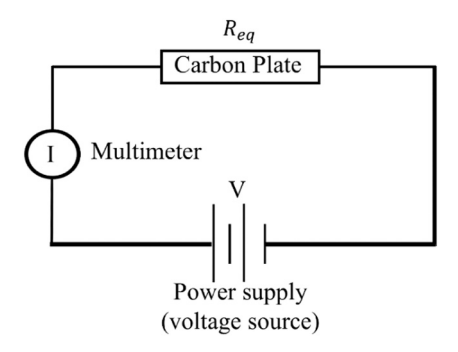


Fig. 3. the thermal images for four connection methods: a) connecting wires to the plate by bolts and nuts, b) using copper bars between the bolts and the carbon plate, c) using a conductive epoxy adhesive between the copper bar and carbon plate, d) inserting a steel strip in between the carbon layers.



**Fig. 4.** Illustration of the circuit configuration for measurements of the electrical resistance of the composite laminate.

fiber prepreg and fiber content, knowing the resistance of the  $0^{\circ}$  plate allows us to theoretically estimate the resistance for other fiber directions (in case all layers in the laminate have the same fiber orientation). This can be achieved by modifying the effective conductive area (effective cross-section area), which is determined by the product of the effective width and the plate thickness (see Fig. 5). This involves adjusting the length to an effective length, as defined in Eq. 1 [11].

$$\rho = \frac{R_{eq} * A_{eff}}{L_{eq}} \tag{1}$$

Where,  $\rho$  is the resistivity and  $R_{eq}$  is the equivalent resistance,  $A_{eff} = W_{eq} * t$  is the effective conductive cross-section area (t is the thickness of the laminate), and  $L_{eq} = L_P / \cos\theta$  is the length of the plate ( $L_P$  is the distance between the electrodes).

MATLAB code is used to analyze the thermal images of composite plates under electrical stress in order to adjust the effective conductive area by precisely calculating the heated region within the plate and determining its proportion relative to the total area (see Fig. 6). Thus, by providing the resistance values of the 0° and 90° plates, the resistance of

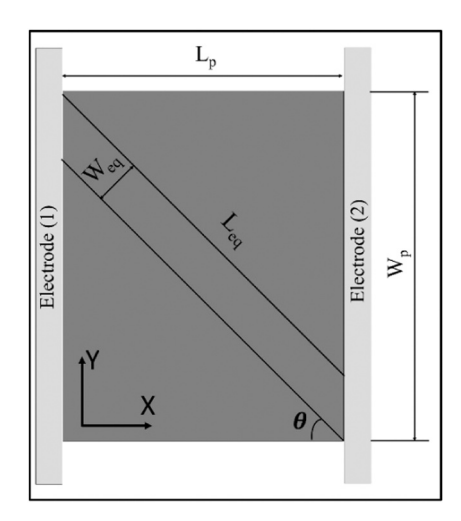
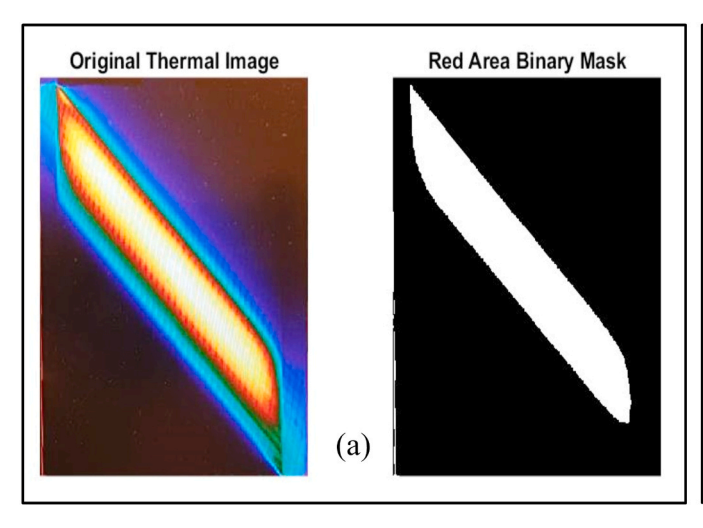


**Fig. 5.** Sketch illustrating the calculation of the effective conductive area in relation to the fiber angle, with  $W_P$  representing the plate width,  $L_P$  the plate length,  $L_{eq}$  the equivalent length,  $W_{eq}$  the equivalent width, and  $\theta$  is the orientation of fibers with respect to the x-coordinate. The electrical path is directed from electrode (1) to electrode (2).

the plate can be calculated theoretically for the other directions and then compared with the obtained experimental results.

As mentioned in the introduction, the fiber alone is responsible for conducting electricity through the composite plate [38]. Theoretical estimation of the plate resistance can be obtained by considering the specific type of carbon fibers used and known fiber volume fraction. The resistivity and diameter of the fiber is available from the datasheet, so it is then possible to calculate the fiber resistance as shown in Eq. 2.

$$R_f = \rho_f \frac{L_f}{A_f} \tag{2}$$



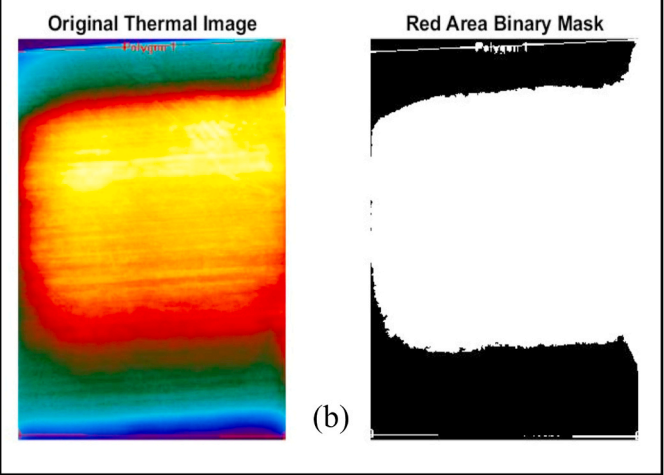


Fig. 6. Images analysed by using MATLAB code to calculate the size of the hot region to determine its ratio with respect to the total size of the plate a) plate with fibers in 45° direction, b) plate with fiber in 0° direction.

The fiber resistance,  $R_f$  is determined by several factors. These factors include the cross-section area of the fiber,  $A_f$ , the fiber length,  $L_f$ , and the fiber resistivity,  $\rho_f$ . The resistivity value from the material datasheet [55] of T700S fiber, used in this study, is  $1.6 \cdot 10^{-3}$   $\Omega$ .cm, and the diameter of the fiber is 7 µm. Consequently, the electrical resistance per unit length is  $4.16 \cdot 10^{+5}$   $\Omega/m$ . To determine the overall electrical resistance of the plate, the count of filaments within the plate should be known. To accurately determine the fiber content (filament count), four samples measuring 2 cm by 2 cm, taken from the plate, were exposed to high temperature (at 450 °C) to burn out the polymer, allowing for the measurement of the average weight of the remaining fibers (62.6 mg). The weight of an individual filament,  $m_b$  can be calculated by multiplying the fiber density as specified in the datasheet as 1.8 g/cm<sup>3</sup> and its volume,  $V_f = A_f \cdot L_f$ . This method not only determines the filament count (45228 filaments, by dividing the total weight of the fibers by  $m_f$ ) but also provides comprehension of the amount of resin surrounding each individual fiber. Thus, the theoretical resistance of a single carbon layer composed exclusively of filaments was calculated to be 0.121  $\Omega$ . This means that the theoretical calculation for [0]<sub>T</sub> plate can estimate the plate's resistance with an error of approximately 9 % in comparison with the experimental value as shown later in Section 4.1.

#### 1.4. Measurements of thermal effects on the plate resistance

To examine the impact of temperature changes on the plate's electrical resistance, measurements were taken at  $23^{\circ}\text{C}$ ,  $80^{\circ}\text{C}$ , and  $100^{\circ}\text{C}$ . Additionally, the resistance was measured at  $-7^{\circ}\text{C}$  to assess how freezing conditions influence the plate's resistance. Plates with dimensions of  $160\times200~\text{mm}^2$ , with different layer orientations (as described later in Table 1) were employed for this investigation. The plate was connected to a power supply, and a thermocouple was

attached to its surface to precisely measure the temperature. The plate was then placed in an oven and heated to 50°C (see Fig. 7). After reaching this temperature, different voltages were applied, and the corresponding currents were recorded, as explained in Section 2.1. The same technique was repeated for 80 °C, 100 °C, and -7 °C but in the case of -7 °C the plate was put inside the freezer, and after the temperature stabilized the resistance was measured.

# 1.5. Measurements of the damage effects on the plate resistance and heat distribution

This section will examine the effect of the damage within plates on the electrical resistance and temperature distribution. Four different laminates  $[0_2]_T,\ [0_3]_T,\ [90/0]_T,\ and\ [\pm 45]_T$  will be studied under various damage scenarios. The damage will be simulated using rectangular cutout areas of varying dimensions, as detailed later in the text, to simulate practical damage scenarios. In case of  $[90/0]_T$  only the 90 layer is assumed to be damaged and the  $0^\circ$  layer is unchanged. For the two-layer plates  $([0_2]_T,\ [\pm 45]_T)$ , two scenarios are considered: 1) a single layer is removed by the cutout and the second ply remains intact; 2) both layers are removed by the cutout, resulting in a rectangular hole representing damage through the entire laminate. For the three-layer plates, also two scenarios are evaluated: 1) only one layer is damaged; 2) two layers are damaged.

In case of one layer damage, the cutout size is equivalent to onequarter of the plate's width and 30 % from the length of the plate, measuring 50 mm by 50 mm. While in case when both layers are damaged, each layer has a different cutout size because the overlap is required in order to get good contact between the patch layer and the plate that will be repaired. Thus, the lower layer has a cutout size of 70 mm\*50 mm and the upper layer has a cutout size of 50 mm\*50 mm,

**Table1**CFRP and GFRP mechanical properties.

CFRP unidirectional lamin	a [56]			
$E_1=113.6\ GPa$	$G_{12} = 4 \text{ GPa}$	$v_{12} = 0.36$	$\alpha_1 = -0.9 \times 10^{-6}~1/K$	$ER_1 = 3.778E{-}05~\Omega{\cdot}m$
$E_2 = 7.7 \text{ GPa}$	$G_{13} = 4 \text{ GPa}$	$v_{13} = 0.36$	$\alpha_2=27\times 10^{-6}~1/K$	$ER_2 = 0.074595~\Omega \cdot m$
$E_3 = 7.7 \text{ GPa}$		$v_{23} = 0.027$	$\alpha_3=27\times 10^{-6}~1/\textrm{K}$	$ER_2 = 0.074595 \ \Omega \cdot m$
GFRP unidirectional lamin	a [57]			
$E_1 = 40 \text{ GPa}$	$G_{12} = 4 \text{ GPa}$	$v_{12}=0.25$	$\alpha_1=6\times 10^{-6}~1/K$	$ER_1 = 1E14 \ \Omega{\cdot}m$
$E_2 = 8 \text{ GPa}$	$G_{13} = 4 \text{ GPa}$	$v_{13} = 0.25$	$\alpha_2 = 35 \times 10^{-6} \text{ 1/K}$	$ER_2 = 1E14 \Omega \cdot m$
$E_3 = 8 \text{ GPa}$		$v_{23} = 0.45$	$\alpha_3=35\times 10^{-6}~1/\textrm{K}$	$ER_2 = 1E14 \ \Omega {\cdot} m$

 $(1\hbox{-along the fiber direction, 2-transverse to the fiber direction, 3-out-of-plane direction, ER-\ electrical\ resistivity).$ 



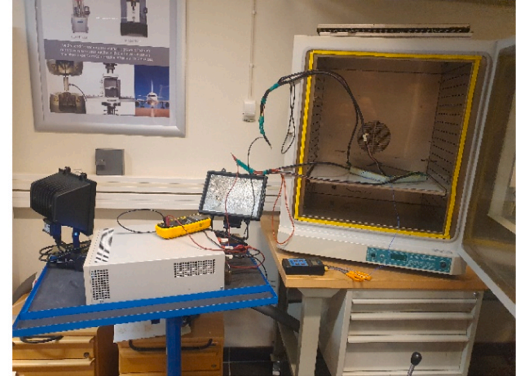


Fig. 7. Setup for electrical resistance measurement (see Fig. 4) at elevated temperatures. Overall view (on the left) with laminate placed in the oven (on the right).

which leaves 10 mm for overlap on two edges, as shown in Fig. 8. The same manufacturing procedure described earlier for plate fabrication in Section 2 was followed. Specifically, the patch layer was positioned over the cutout in the original plate, then placed in a hot press at 130 °C and

Electrode (1)

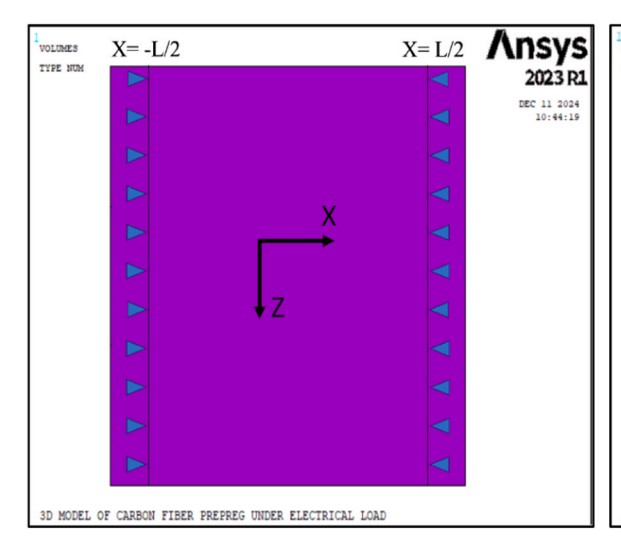
Electrode (2)

**Fig. 8.** Schematic of a plate with two cutouts representing the damaged area in both layers, the electrical path is directed from electrode (1) to electrode (2).

 $3\ \mathrm{bar}$  for  $30\ \mathrm{min},$  ensuring complete matrix curing and proper bonding to the surrounding laminate.

#### 1.6. Finite element model

A 3D numerical analysis was performed to evaluate the thermal and electrical performance of a rectangular carbon fiber composite plate. The analysis considered varying fiber orientations in different layers and explored various plate dimensions. The voltage was applied to simulate electrical field. The simulations were done by using a commercial FEM package ANSYS 2023 R1 (utilizing APDL codes). A 3D coupled-field solid element (SOLID226) [55], containing twenty nodes, was utilized for the analysis of coupled electro-thermo-mechanical behavior to capture the multi-physics response of the carbon fiber laminates under electrical loading. A uniform mesh with constant element size was generated across the entire plate. Convergence of the results was verified by studying mesh size dependence on temperature predictions. In this simulation, two different materials are used through the thickness of the plate in order to simulate the real scenario of the turbine blades which consists of glass and carbon fiber layers. The simulation employs the same geometry and dimensions as the test specimens, using boundary conditions that replicate those in the experiment: an electrical load is applied at both ends of the plate, corresponding to the electrode positions in the experimental setup at X = -L/2 and X = L/2 (as presented in Fig. 9). Surface loads (thermal convection) are applied to the outer areas of the plate, which experience convection with the surrounding air (see Fig. 9). Mechanical, thermal, and electrical properties (as shown in Table 1) are provided for the standard linear orthotropic material model



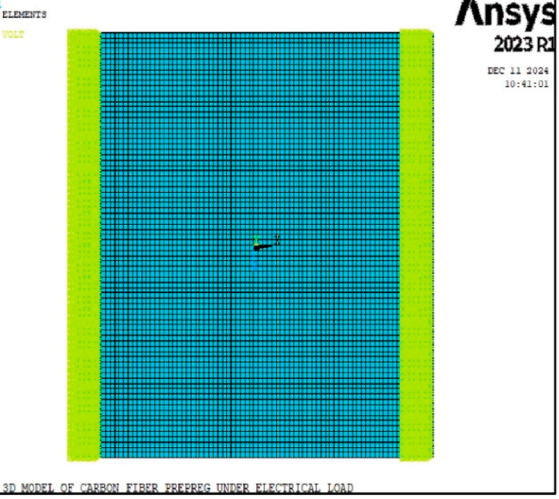


Fig. 9. Configuration of the FE model (left) and mesh for the entire plate (right), the voltage is applied on the green area to ensure it is representative of experiments.

within ANSYS, enabling accurate simulation. Mesh sensitivity was evaluated using three different mesh sizes: 13120, 51840, and 80800 elements. The results demonstrated full convergence at 80800 elements, while at 51840 elements, the error was already within 0.1 %. Considering computational efficiency, reducing computation time by roughly a factor of 10, the mesh with 51840 elements was selected for subsequent simulations.

#### 2. Results and discussion

The section presents the results of this study, including the effects of fiber orientation, the impact of plate temperature on resistance, heat distribution in laminates with different layups, and the influence of damage on both resistance and heat distribution. Additionally, the heat transfer through damaged plates and the effect of plate size on resistance and heat distribution are examined. The analysis emphasizes the comparison of experimental results for electrical resistance, temperature generation, and heat distribution within the carbon layer of the flat plate. A comparison between experimental and numerical results for these parameters is also provided. The plate configurations used in each investigation are detailed in Table 2.

The direct measurement of the plate resistance by multi-meter was not feasible due to low accuracy and instability of measurements. Instead, various voltage values are applied to the plate, and the corresponding current is measured (as shown in Fig. 4). By plotting the relationship between voltage and current, a linear slope of the graph will represent the equivalent Ohmic resistance i.e. sample plate resistance, as shown in Fig. 10. In order to ensure accuracy in determining the plate resistance, the resistance value of each plate has been adjusted by subtracting the wire resistance to get the actual plate resistance (since wires are part of the circuit and their resistance is included in the measurement).

#### 2.1. Impact of fiber orientation on plate resistance

This section discusses how the electrical resistance varies with different orientations of carbon layers. The measurement is done according to the explanation in Section 2.1. The experimental results for the electrical resistance of various plates are shown in Table 3.

The plate with a  $[0_2]_T$  layup demonstrated the lowest electrical resistance among all configurations. The cross-ply laminates,  $[\pm 45]_T$  and  $[0/90]_T$ , exhibited electrical resistances 80 % and 97 % higher, respectively, than the unidirectional  $[0_2]_T$  lamina. The off-axis  $[45]_T$  plate had a resistance approximately eight times higher than the  $[0]_T$  plate. This result is consistent with expectations, as the fiber length in the  $[45]_T$  configuration increases by 60 % compared to 0-plate, while the cross-sectional area decreases by 80 %, leading to an expected rise in resistance according to Eq. 1. Meanwhile, the quasi-isotropic laminate  $[0/45/-45/90]_T$  showed only a 2 % difference in resistance, though it's important to consider the impact of any variations in the plate's cross-sectional area. To eliminate the impact of changes in the plate's cross-sectional area (due to changes in the thickness of the plate), the

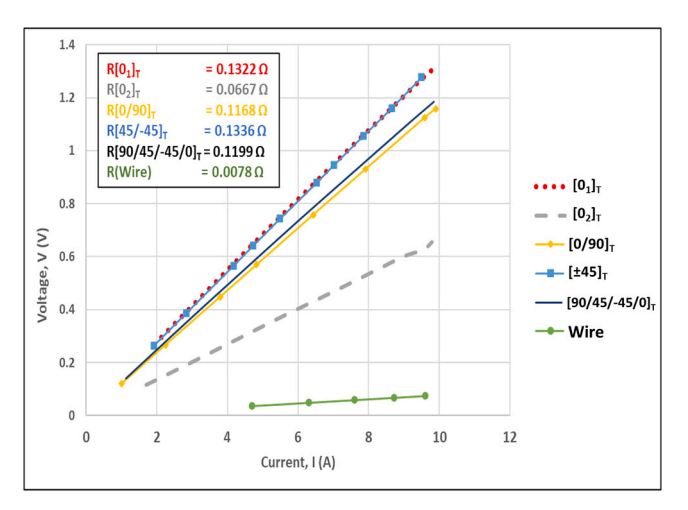


**Fig. 10.** Comparison of electrical resistance for plates with different fiber orientations: resistance values derived from line slopes are corrected for wire resistance.

**Table 3**Measured electrical resistance for different fiber orientations.

Stacking sequence*	Thickness (mm)	Width (mm)	Distance between the electrodes (mm)	Resistance (ohm)
[0] <sub>T</sub>	0.25	200	160	0.1322
[45] <sub>T</sub>	0.25	200	160	1.0658
$[0_2]_T$	0.5	200	160	0.0647
$[90_2]_T$	0.5	200	160	134.37
$[0/90]_{T}$	0.5	200	160	0.1275
$[45/-45]_{\rm T}$	0.5	200	160	0.1185
$[0/45/-45/90]_{\mathrm{T}}$	1	200	160	0.0653

Index "T" stands for "Total"

resistance values should be normalized with respect to the thickness of the plate. After applying this normalization, the difference in resistance compares to 0-plate increases from 2 % to 102 %. Notably, the  $[90_2]_T$  layer exhibited an extremely high electrical resistance, roughly 2000 times greater than that of the  $[0_2]_T$  laminate. This result is expected, as the  $[90_2]_T$  layer, in theory, should block any current flow (the fibers are insulated by the matrix). However, small misalignments and fiber waviness create contact points along the length of the fibers, allowing some current to flow even in a  $90^\circ$  orientation. This inter-fiber interaction also explains why the electrical conductance in the out-of-plane direction closely resembles that in the transverse direction, which contrasts with the findings of [41].

#### 2.2. Temperature distribution in laminates with varying layups

Five different plates with different layer orientations (as presented in

 Table 2

 Classification of plates used in different investigations.

Study Parameters	Plate typ	ne .							
Study Furameters	[0] <sub>T</sub>	[0 <sub>2</sub> ] <sub>T</sub>	[0 <sub>3</sub> ] <sub>T</sub>	[0/90] <sub>T</sub>	[45] <sub>T</sub>	[±45] <sub>T</sub>	[90 <sub>2</sub> ] <sub>T</sub>	[0/±45/90] <sub>T</sub>	[±45] <sub>T</sub> sep
Fiber orientation R	X	Х		X	X	Х	X	Х	
Fiber orientation T		X		X		X	X	X	X
Change of T on R		X		X		X	X	X	X
Structural damage on R and T		X	X	X		X			
Plate size on T		X			X				
Repair quality		X	X	X		X			
Numerical simulations		X		X		X	X	X	X

R: Resistance

T: Temperature

Table 1) were used in this investigation in order to estimate the effect of fiber orientation on the heating efficiency of the plate. For consistency, all tests were conducted by applying 2 V and waiting until a steady-state temperature was achieved. Fig. 11 illustrates that the  $[0_2]_T$  plate

achieves the highest maximum temperature compared to other layup configurations under similar conditions. This occurs because the lower electrical resistance allows greater current flow, leading to more power being dissipated as heat (as described by Eq. 3, where *P* is the power that

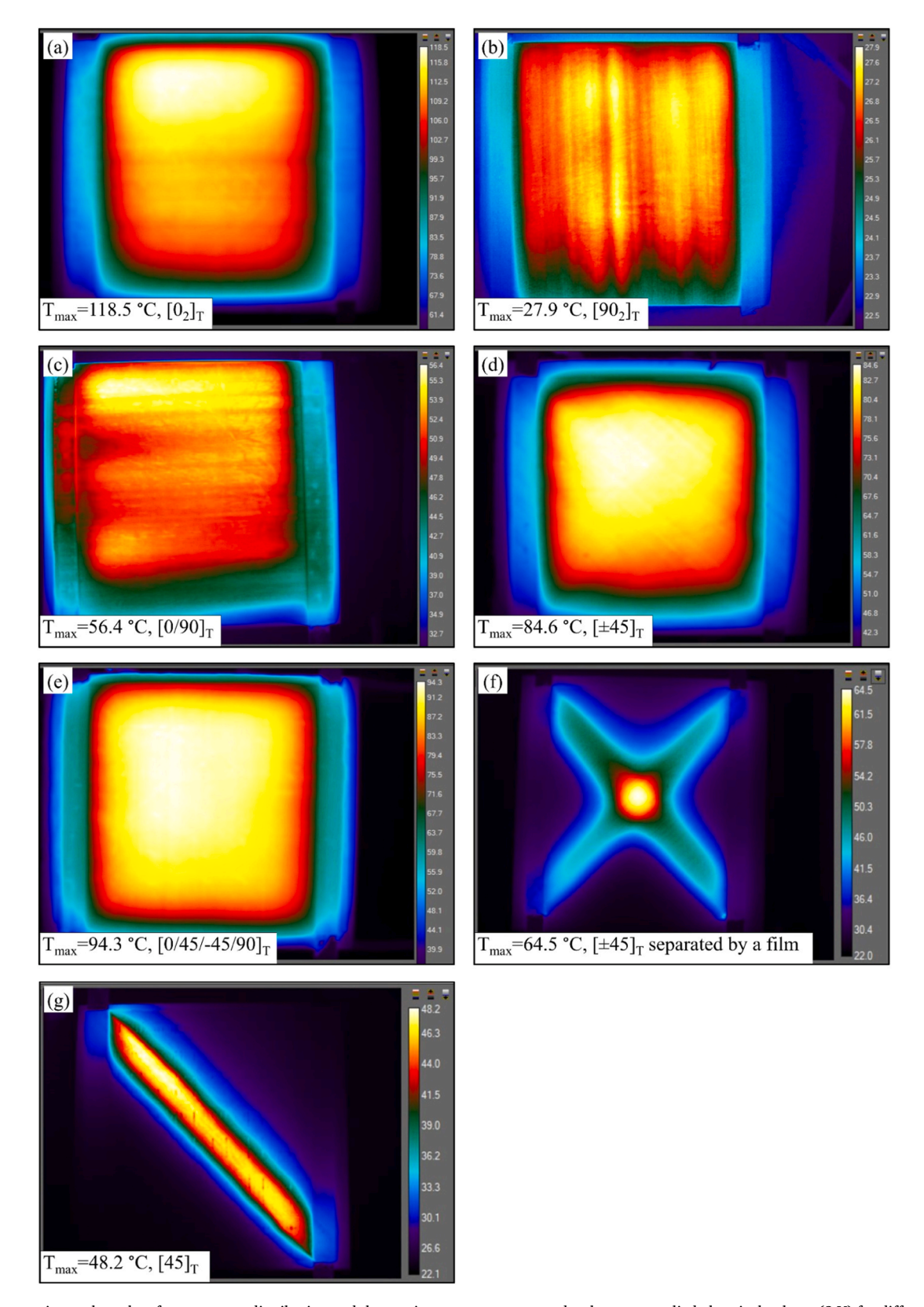


Fig. 11. The experimental results of temperature distribution and the maximum temperature under the same applied electrical voltage (2 V) for different laminates: a)  $[0_2]_T$ , b)  $[90_2]_T$ , c)  $[0/90]_T$ , d)  $[\pm 45]_T$ , e)  $[0/45/-45/90]_T$ , f)  $[\pm 45]_T$  separated by a film, g)  $[45]_T$  monoclinic materials.

generates heat, *R* is the resistance, and *V* is the applied voltage).

$$P = V^2/R \tag{3}$$

Moreover, as seen in Fig. 11, the temperature rise in the  $[0_2]_T$  plate was nearly double that of the [0/90]<sub>T</sub> plate under the same applied voltage. It was also about 40 % greater than the [45/-45]<sub>T</sub> plate and 4.5 times higher than the  $[90_2]_T$  plate. However, the  $[0_2]_T$  plate's temperature increase was only 25 % higher than that of the quasi-isotropic [0/  $\,$ 45/-45/90]<sub>T</sub> laminate, likely due to the greater number of contact points between the fibers through the thickness. At the same time, more layers are required to match the temperature of the  $[0_2]_T$  plate. As a result, the [02]<sub>T</sub> plate required significantly less electrical current, about 25 % of the current needed for other layups to achieve the same temperature increase. Additionally, as shown in Fig. 11-f, when the two layers oriented at 45° were separated by a film during the manufacturing, the temperature increased significantly at the plate's center, when fibers from both layers crossed the same area. However, the temperature remained lower than that of the  $[\pm 45]_T$  configuration without the separating film between the layers. The film prevented direct fiber contact through the thickness, reducing the effective flow area and consequently decreasing heat generation within the plate. The temperature map shows that only the fibers connected to both electrodes created a closed circuit and generated heat, while the rest of the plate remained cool, unlike the scenario in Fig. 11-d, where the whole plate was uniformly heated. A similar pattern is observed in Fig. 11-g for monoclinic materials, where the temperature is comparable to that in Fig. 11-f, but in Fig. 11-f the center heating more intensely due to both layers being heated simultaneously in the same area.

#### 2.3. The influence of temperature on the resistance of the composite

This section focuses on the effect of surrounding temperature changes on the plate's electrical resistance, four surrounding temperatures were considered  $-7^{\circ}$ C,  $23^{\circ}$ C,  $80^{\circ}$ C, and  $100^{\circ}$ C. The test follows the scenario that is described in subsection 2.3. According to existing literature, the electrical resistance of carbon plates (semiconductors) tends to reduce with the rise in temperature while the electrical resistance of the metal wire increases with increasing temperature. As shown in Table 4, the test results indicate that, as expected, the plate's resistance decreases with increasing temperature (as shown in Fig. 12), although the effect is not highly significant.

Notably, the resistance of the wires themselves (that are used for the measurement) increases with increasing temperature, which reduces the temperature's effect on the overall measured resistance. The plate  $[\pm 45]_T$  exhibited the maximum increase in resistance when it is placed in the freezer, with a rise of  $\sim 3$  %, while the plate  $[0/\pm 45/90]_T$  showed the greatest reduction in resistance when heated, decreasing by  $\sim 6$  %.

### 2.4. Effects of the damage on plate resistance and heat distribution

This section focuses on measuring the electrical resistance of damaged plates to determine how resistance changes in relation to the level of damage. Additionally, the effect of damage on the temperature distribution within the plate will be monitored as described in Section 2.4. In the first case  $[0/90]_T$ , only the  $90^\circ$  layer was damaged, while the

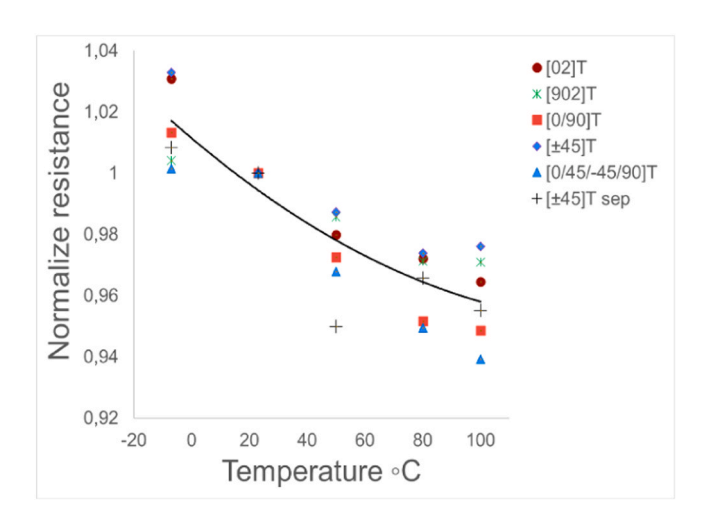


Fig. 12. Impact of temperature variation on the electrical resistance of carbon plates, the resistance values are normalized to the plate's resistance at room temperature ( $\approx$ 23°C).

0° layer remained undamaged. It was expected that the resistance would not change, as the 0° layer is responsible for the current flow between the electrodes (this is true only if the two layers are separated by a film or similar material to prevent contact between them through the thickness), not the 90° layers. However, a difference of around 13 % lower than the resistance of the original plate was observed in the experiment (see Table 4), which could not be attributed to measurement error. This can be explained by the fact that fibers in the 90° layers create multiple contact points through the thickness direction, and when part of the layer is damaged, number of these points is reduced, affecting the resistance. Additionally, the resistance decreased in proportion to the reduction in the effective conductive area. The effective conductive area was reduced by 12.5 %, and the resistance changed by approximately the same amount. In the second case  $[0_2]_T$ , when only one 0° layer is damaged, the effective conductive area is reduced by 12.5 %, and the electrical resistance increases by 1 % (as shown in Table 5).

However, when both layers are damaged, with a 25 % reduction in effective conductive area, the electrical resistance increases by 18 %. This indicates that damage to a single  $0^{\circ}$  layer has little effect on the resistance. However, when the damage extends through the entire thickness, the resistance is significantly affected, corresponding to approximately 70 % of the damage percentage (25 % reduction in effective conductive area). In the case of a  $[\pm 45]_T$  configuration, when the damage affects 12.5 % of the plate's effective conductive area (only

**Table 5**Electrical resistance across various fiber orientations under different damage scenarios.

Stacking sequence	Experimen	Experimental value of the resistance ( $\Omega$ )					
	[0 <sub>2</sub> ] <sub>T</sub>	[0 <sub>3</sub> ] <sub>T</sub>	$[0/90]_{T}$	[±45] <sub>T</sub>			
No damage	0.0647	0.0466	0.1275	0.1188			
One cutout layer	0.0653	0.0599	0.1108	0.1793			
Two-cutout layer	0.0775	0.0623	-	0.2321			

**Table 4**Electrical resistance for different fiber orientations at different temperatures.

Temp. (°C)	Resistance (S	Resistance ( $\Omega$ )							
	[0 <sub>2</sub> ] <sub>T</sub>	$[0/90]_{T}$	[±45] <sub>T</sub>	[90 <sub>2</sub> ] <sub>T</sub>	$[0/\pm 45/90]_{T}$	[±45] <sub>T</sub> sep	Wire		
<del>-7</del>	0.0667	0.1292	0.1224	134.93	0.0654	0.5000	0.0074		
23	0.0647	0.1275	0.1185	134.37	0.0653	0.4959	0.0076		
50	0.0634	0.1240	0.1170	132.45	0.0632	0.4710	0.0077		
80	0.0629	0.1213	0.1154	130.49	0.0620	0.4789	0.0078		
100	0.0624	0.1209	0.1150	130.46	0.0613	0.4736	0.0079		

one layer is damaged), the resistance increases by 51 %. When the cutout area expands to 25 % of the effective conductive area (two layers are damaged), the resistance rises by 95 %. This increase is quite significant, as the plate's resistance nearly doubles. Additionally, for the  $[0_3]_T$  configuration, when 8 % of the effective area is damaged (with only one layer affected), the electrical resistance increases by 28.5 %. When the damaged area extends to 16 % (with two layers damaged), the resistance increases by 34 %. It can be concluded from the results that the optimal scenario is using only 0° layers to manufacture the heating layer for turbine blades, as the damage has the smallest impact on plate resistance.

The resistance of plates with different stacking sequences and damage scenarios can be predicted using experimental resistance results from undamaged  $[0]_T$ ,  $[90]_T$ , and  $[\pm 45]_T$  plates. The resistance of individual layers for  $0^\circ$  and  $90^\circ$  fiber orientations can be used to estimate the resistance for plates with different layups. However, for the  $\pm 45^\circ$  orientation, resistance must be provided as a combined value for both  $\pm 45^\circ$ , since the resistance cannot be accurately calculated by separating the  $45^\circ$  and  $-45^\circ$  orientations. The calculation results are shown in Table 6. For undamaged plates with different  $0^\circ$  and  $0^\circ/90^\circ$  layups, the

Table 6
Predicted value of electrical resistance across various fiber orientations under different damage scenarios.

Stacking sequence	Predicted Resistance (Ω)						
	$[0_2]_{T}$	[0 <sub>3</sub> ] <sub>T</sub>	[0/90] <sub>T</sub>	[±45] <sub>T</sub>			
No damage	0.0661	0.0441	0.1321	_			
One cutout layer	0.0751	0.0479	0.1322				
Two-cutout layer	0.0870	0.0537					
Three-cutout layer	-	0.0580					

resistance can be predicted with an error range of 2–5 %. For damaged plates, the error increases to be from 8 % to 16 %. On the other hand, the resistance of plates with  $\pm 45^{\circ}$  orientations cannot be predicted through calculations unless the layers are separated by a film, preventing contact between them. This indicates significant interaction between the layers, which cannot be neglected.

The maximum temperature of the undamaged plate is 120°C (see Fig. 13-a), observed in the plate with the  $[0_3]_T$  stacking sequence, followed by the plates with  $[0_2]_T$  and  $[\pm 45]_T$  stacking sequences, which reached maximum temperatures of 105.3°C (see Figs. 14-a) and 84.6°C (see Fig. 15-a), respectively. These values are consistent with expectations, as the  $[0_3]_T$  plate has the lowest resistance compared to the others. As can be seen in Figs. (13, 14, and 15) the maximum temperature is reduced with the increase in the damage percentage. The maximum temperature for the plates with one layer damaged is reduced by 20 %, 13 %, and 13 % for  $[0_3]_T$ ,  $[0_2]_T$ , and  $[\pm 45]_T$  respectively. At the same time, the damage percentage for those plates are the following 8 %, 12.5 %, and 12.5 % respectively. The maximum temperature for the [0<sub>3</sub>]<sub>T</sub> plate with two damaged layers (Fig. 13-c) is the same as for the plate with only one damaged layer (Fig. 13-b), although the temperature in the damaged area is lower. In contrast, for the  $[0_2]_T$  plate, the maximum temperature decreases by 3.5 % when two layers are damaged compared to when only one layer is damaged. As shown in the figures, when the plate is damaged through the entire thickness, no current flows through the damaged area which means that the electrical circuit is cut completely in the damaged region. However, the thermal distribution in the plate with a  $0^{\circ}$  layer orientation is more uniform compared to that of the plate with a 45° orientation.

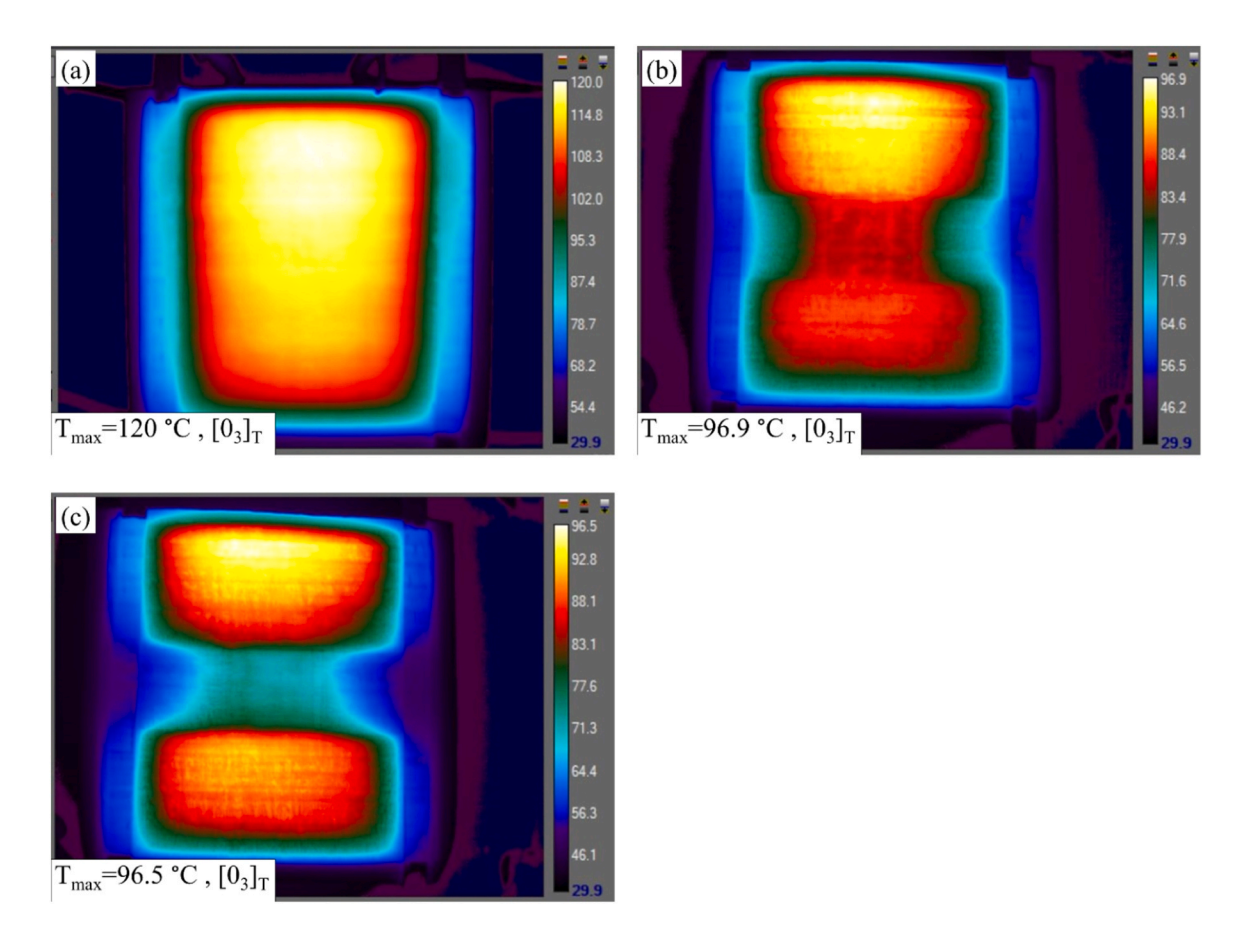


Fig. 13. Temperature distribution for the  $[0_3]_T$  plate under different damage scenarios: a) undamaged plate, b) one cutout layer with two intact layers, and c) two cutout layers with one intact layer.

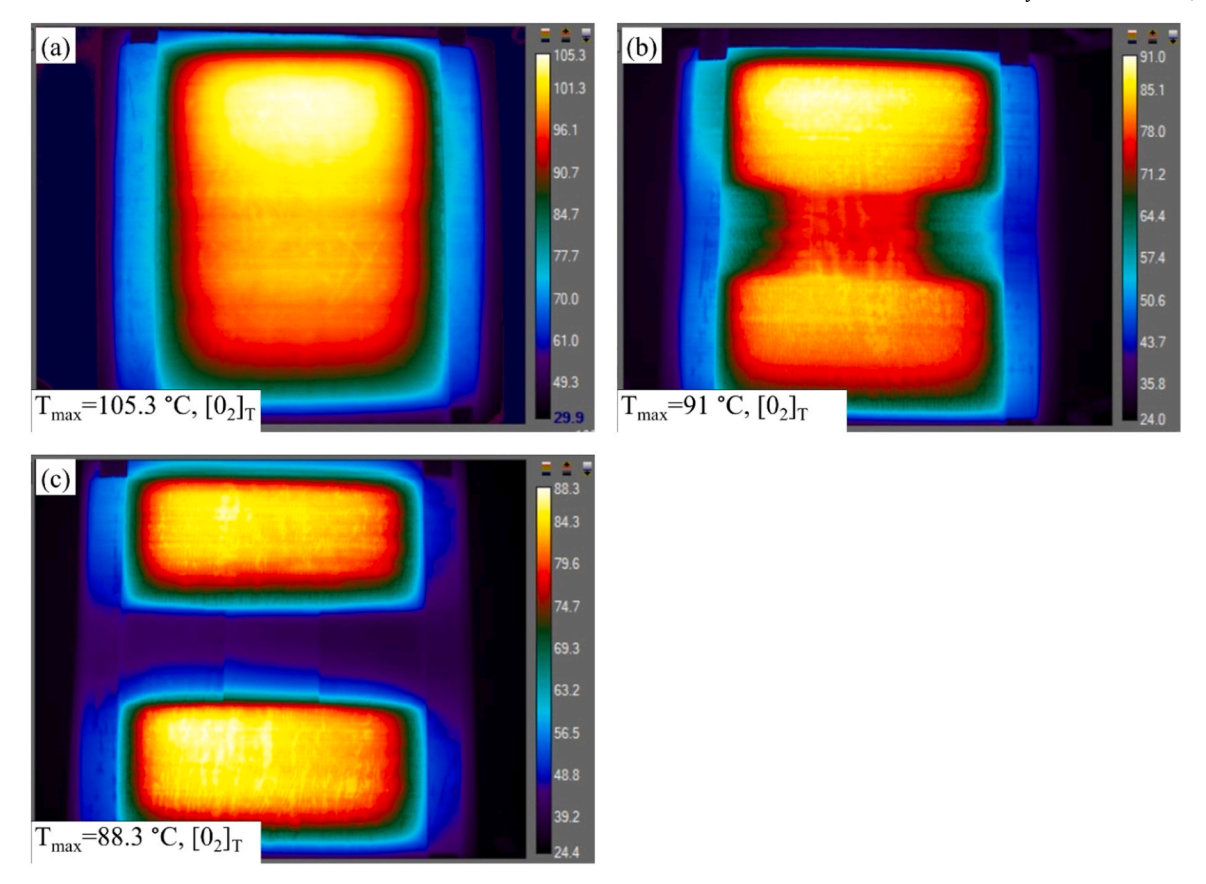


Fig. 14. Temperature distribution for the  $[0_2]_T$  plate under different damage scenarios: a) undamaged plate, b) one cutout layer with one intact layer, and c) two cutout layers.

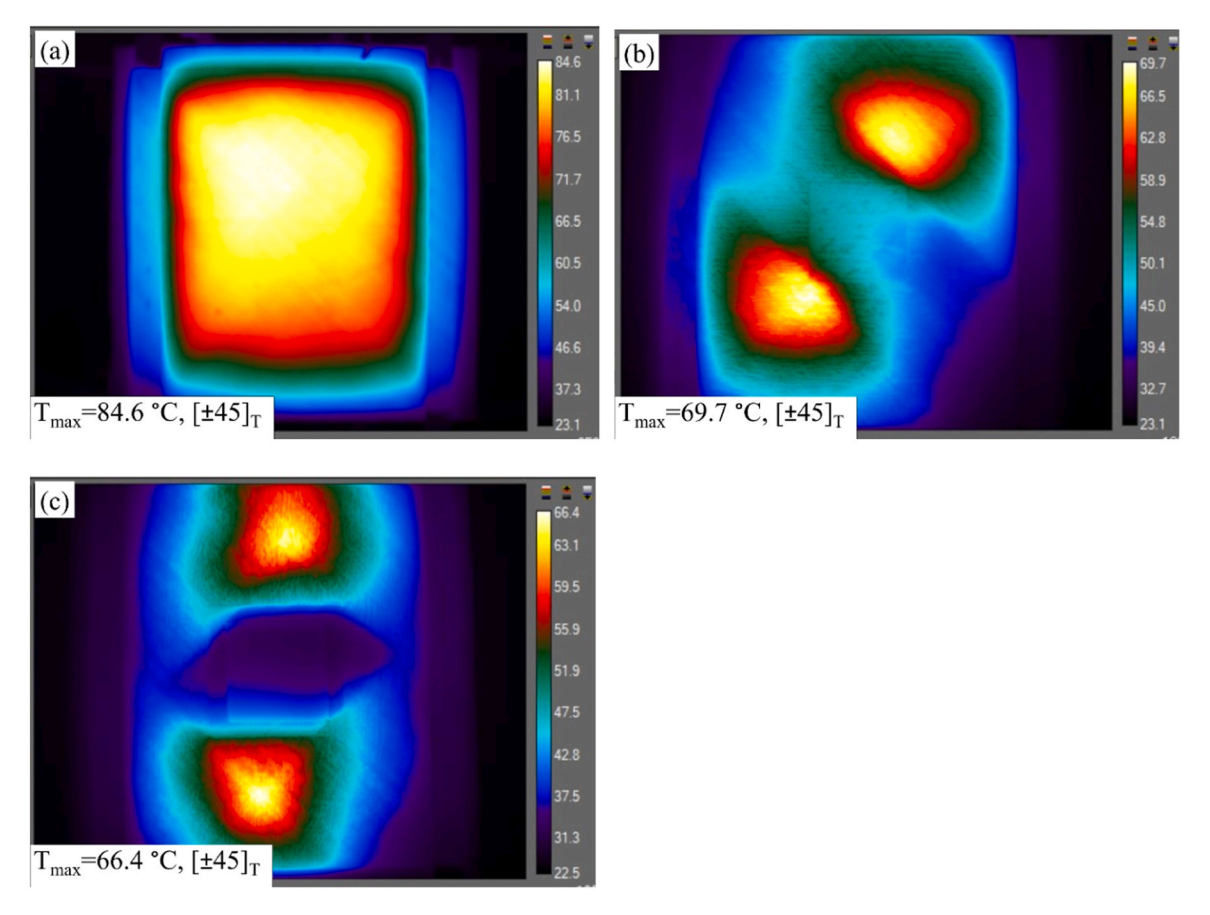


Fig. 15. Temperature distribution for the  $[\pm 45]_T$  plate under different damage scenarios: a) undamaged plate, b) one cutout layer with one intact layer, and c) two cutout layers.

# 2.5. Impact of plate size on maximum temperature and thermal distribution

This section examines the comparison of five carbon fiber composite plates with varying widths. Two plates feature  $0^\circ$  layers, while the other three have  $45^\circ$  fiber orientations. The experimental results for the  $0^\circ$  layer plates are shown in Fig. 16. The findings reveal that increasing the length of the plate by 80 % increases the resistance by 65 %, while the maximum temperature drops by 53 % compared to the original 160 mm plate. This outcome is expected, as the cross-sectional area for current flow remains constant, and the longer fiber length contributes to the rise in resistance.

In the case of plates with 45° fiber orientations (monoclinic materials), three different widths (160 mm, 200 mm, 285 mm) were tested to observe the differences in thermal distribution. As shown in Fig. 17-b, when the plate's width and length are equal, the current flows through a very narrow line-like area, resulting in a high temperature concentrated in a small hot spot. As the difference between the plate's length and width increases, the width of the heated area also expands. The width of the current flow area corresponds to the difference between the plate's width and length, as seen in Figs. 17-a and 17-c. As expected, the temperature increased as the flow area expanded, as shown in Fig. 17. This aligns with previous findings, where the reduction in resistance with a larger flow area led to increased heat generation, as explained by Eq. 3.

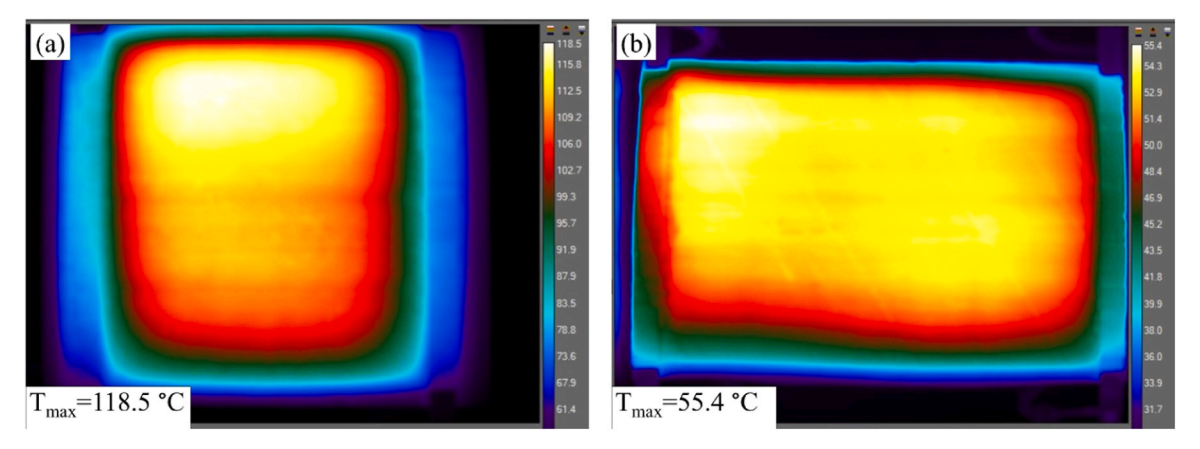


Fig. 16. Experimental results of thermal distribution and maximum temperature for  $[0_2]_T$  at 2 V with varying plate length (electrode distances): a) 160 mm, b) 285 mm.

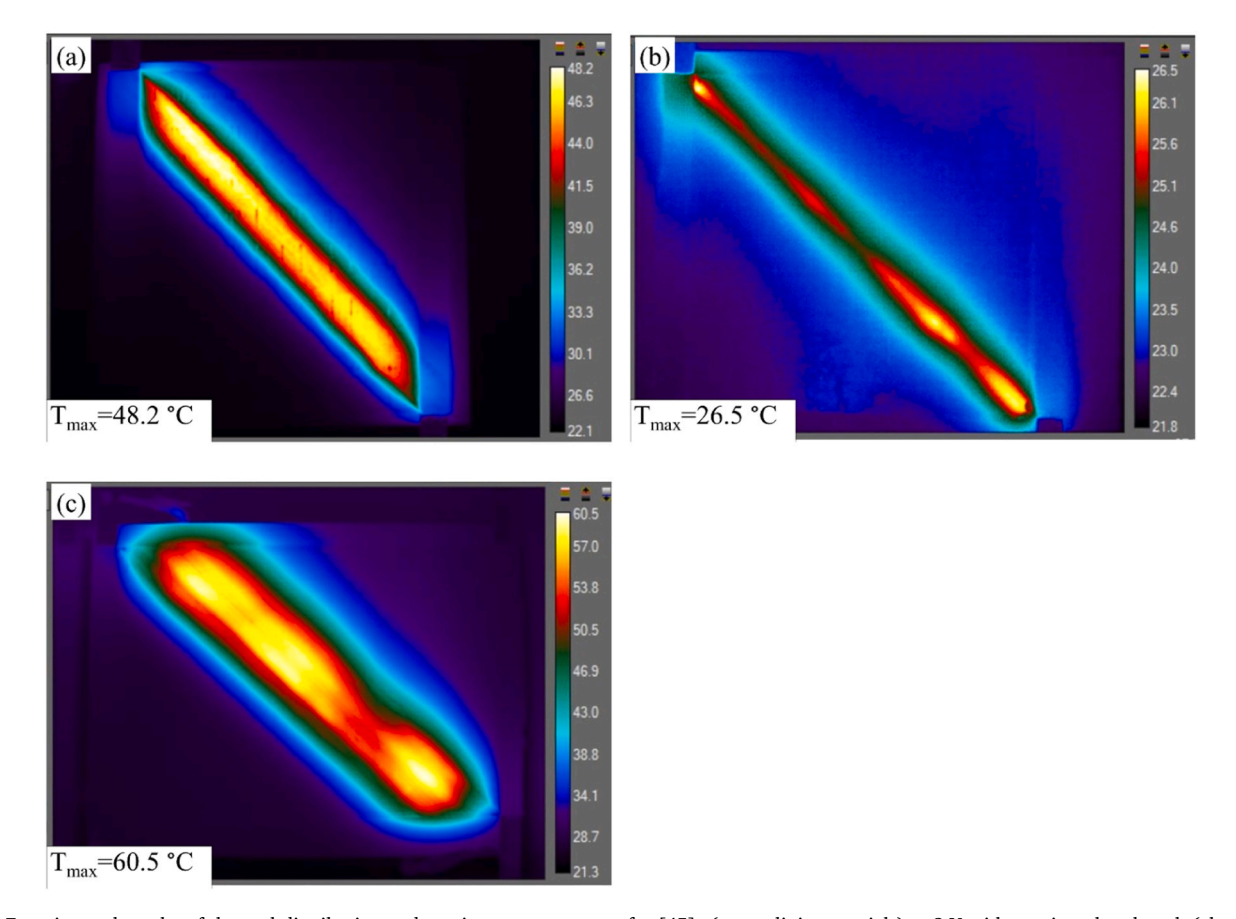


Fig. 17. Experimental results of thermal distribution and maximum temperature for [45]<sub>T</sub> (monoclinic materials) at 2 V with varying plate length (electrode distances): a) 160 mm, b) 200 mm, and c) 285 mm.

As a result, the  $0^{\circ}$  fiber orientation provides a much better flow area compared to other configurations.

# 2.6. Evaluation of repair quality and performance for different damage scenarios

In this section, several tests were done to evaluate the quality of the repair in terms of electrical resistance, and heat generation (temperature distribution). Several scenarios of patch configuration will be discussed here. Two different damage scenarios (one damaged layer and two damaged layers) will be presented for four different plates (see Table 2). As shown in Fig. 18, for the  $[0_2]_T$  configuration with one damaged (cutout) layer, the thermal distribution after repair nearly returns to that of the undamaged plate (see Fig. 14-a), with a reduction in maximum temperature of around 15 %. When the damage extends through the laminate, as shown in Fig. 19 for  $[0_2]_T$  configuration with two damaged layers, the entire carbon layer needs to be removed from the glass fiber. In this case, achieving good contact in the center of the repairing area can be challenging, and maybe it is necessary to work layer by layer to improve the thermal distribution in that region. However, notwithstanding these challenges, a significant improvement is observed when comparing the

**Table 7**Electrical resistance across various fiber orientations under different repairing scenarios

Stacking sequence	Experimental Resistance (Ω)				
	$[0_2]_{T}$	$[0_3]_{T}$	[0/90] <sub>T</sub>	[±45] <sub>T</sub>	
No damage	0.0647	0.0466	0.1275	0.1188	
One layer was repaired	0.0652	0.0499	0.1223	0.1617	
Two-layer were repaired in one step	0.0681	-	-	0.1462	
Two-layer were repaired in two steps	-	0.0503	-	0.1508	

damaged and repaired plates. In the damaged state, the current is completely interrupted in the cutout area, whereas after repair, current flow is restored, though not at the same level of efficiency as in an undamaged plate. Based on the recorded data, the resistance of the plate with one cutout layer (see Table 5) can be significantly improved after repair, returning it to nearly the same level as the undamaged plate, with only a 1 % increase in resistance, as shown in Table 7. Similarly, the plate with two cutout layers also shows a significant improvement after repair when compared to its pre-repair resistance (see Table 5). However, it has a slightly higher resistance than the undamaged plate, with an increase of approximately 5 % (see Table 7).

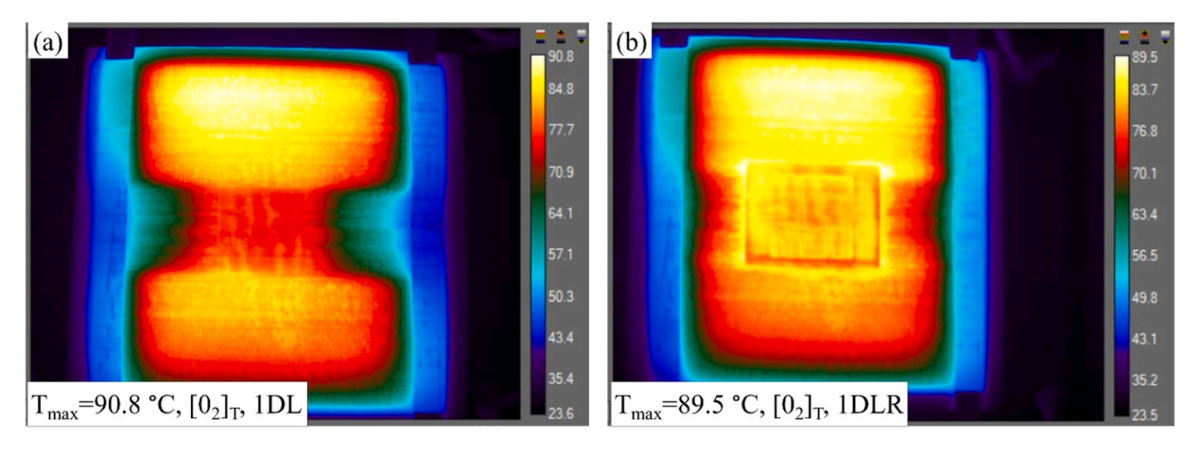


Fig. 18. Experimental results of thermal distribution and maximum temperature for  $[0_2]_T$  with one cutout layer and one layer intact at 2 V: a) damaged plate, b) plate after repair.

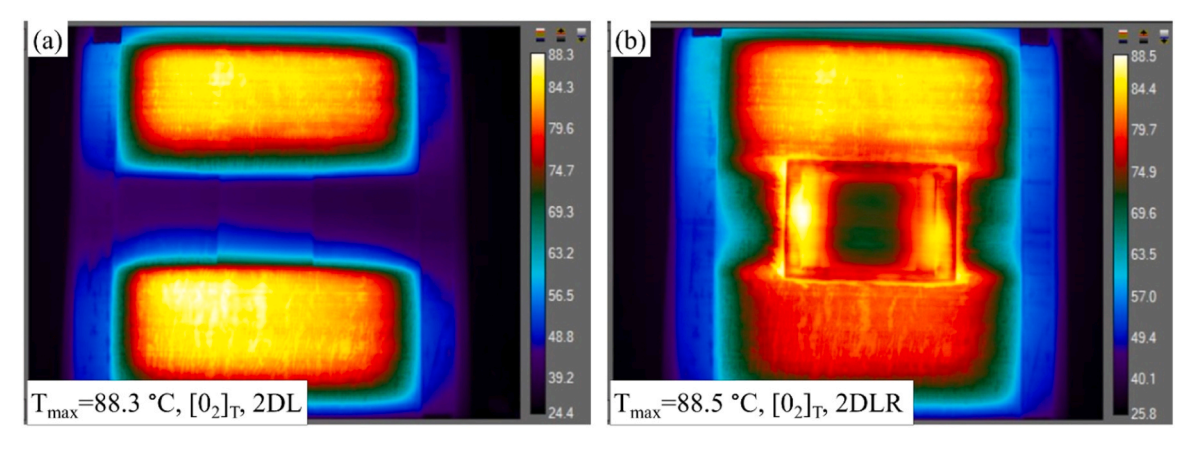


Fig. 19. Experimental results of thermal distribution and maximum temperature for  $[0_2]_T$  with two cutout layers (damage through the whole thickness) at 2 V: a) damaged plate, b) plate after repair.

For a plate with three  $0^\circ$  layers, two damage scenarios are considered: one cutout layer and two cutout layers (the repairing is done in two steps "layer by layer"). In both cases, the repair results in excellent contact and thermal distribution, closely resembling that of the undamaged plate, with a slight decrease in maximum temperature. As shown in Figs. 20 and 21, the maximum temperature decreases by approximately 17 % when repairing a plate with one layer damaged, and by about 25 % when repairing a plate with two cutout layers. The electrical resistance of the plate with one cutout layer can be significantly improved after repair, reducing the resistance by 17 % compared to the damaged state (see Table 5) and bringing it within 7 % of the undamaged plate's resistance (see Table 7). In the case of two cutout layers, where the repair is performed in two steps, the resistance can be improved by 20 % (see Table 5), resulting in an overall increase of 7.5 % compared to the undamaged plate (see Table 7).

For the  $[90/0]_T$  configuration with one damaged layer, the  $90^\circ$  layer is damaged, as shown in Fig. 22-a. The results indicate that damage to the  $90^\circ$  layer does not impact the thermal distribution, and the condition before repair is actually better than after repair (see Fig. 22-b). Regarding electrical resistance, damage to the  $90^\circ$  layer reduces the overall resistance. After repair, the resistance remains lower than that of the original undamaged plate (see Tables 5 and 7).

For the  $[\pm 45]_T$  plate configuration, two damage scenarios and corresponding repair approaches are presented: single layer is cutout and repaired in one step; two cutout layers, with repairs conducted in one and two steps. In the case of a single cutout layer, as shown in Fig. 23, the repaired plate presents better thermal distribution (see Fig. 23-b), though there remains a significant difference compared to the undamaged plate (see Fig. 15-a). While the thermal distribution improves, it is still not as good as required. Regarding electrical resistance, there is a

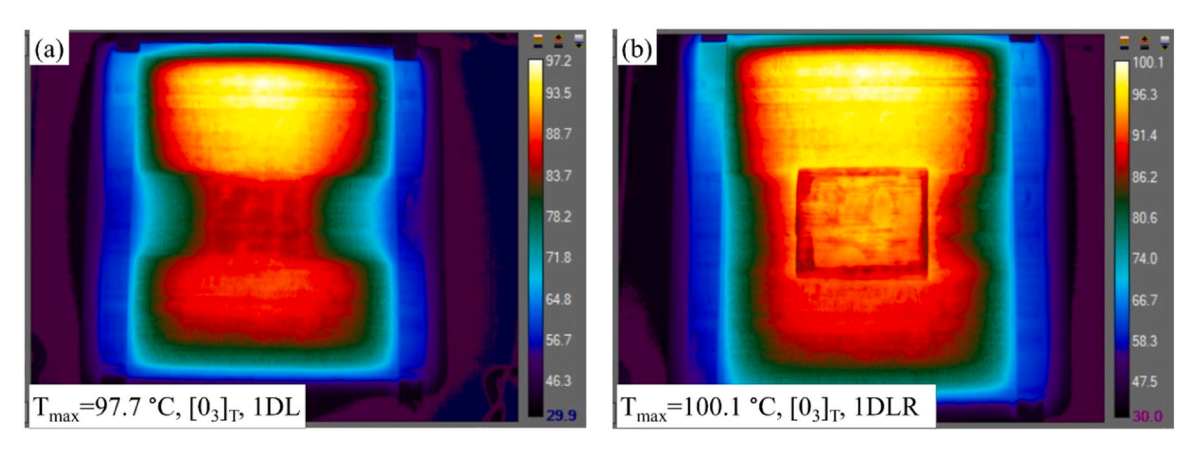


Fig. 20. Experimental results of thermal distribution and maximum temperature for  $[0_3]_T$  with one cutout layer and two cutout layers intact at 2 V: a) damaged plate, b) plate after repair.

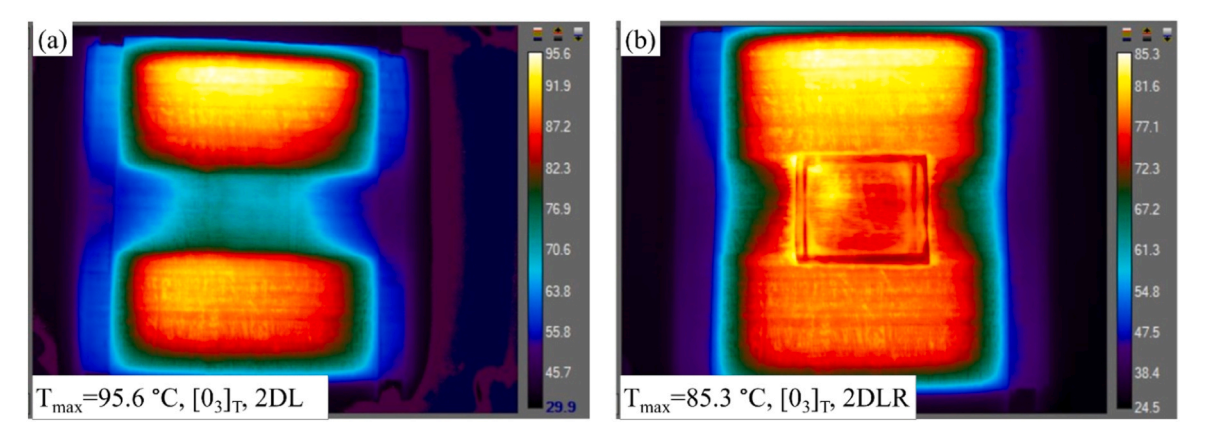


Fig. 21. Experimental results of thermal distribution and maximum temperature for  $[0_3]_T$  with two cutout layers and one layer intact at 2 V: a) damaged plate, b) plate after repair.

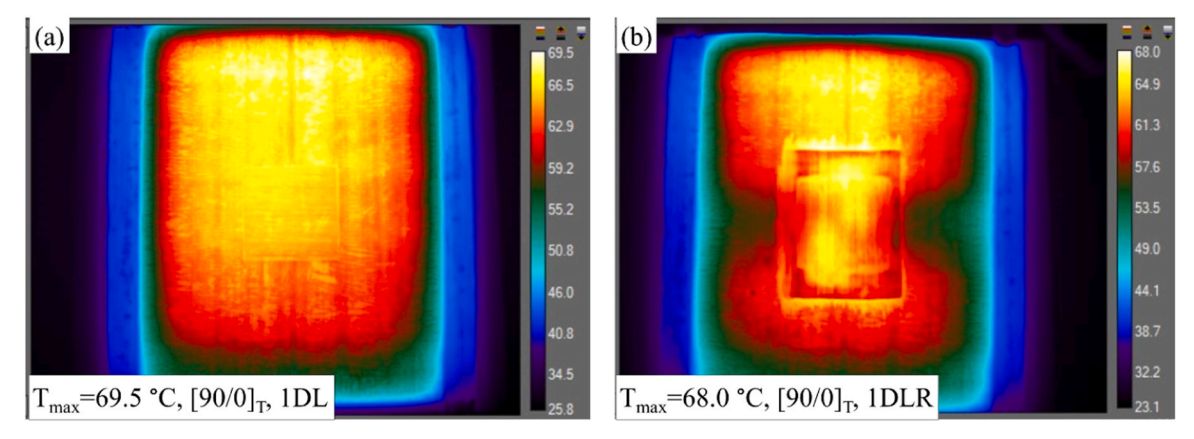


Fig. 22. Experimental results of thermal distribution and maximum temperature for  $[90/0]_T$  with one cutout layer (only  $90^\circ$  layer is damaged) at 2 V: a) damaged plate, b) plate after repair.

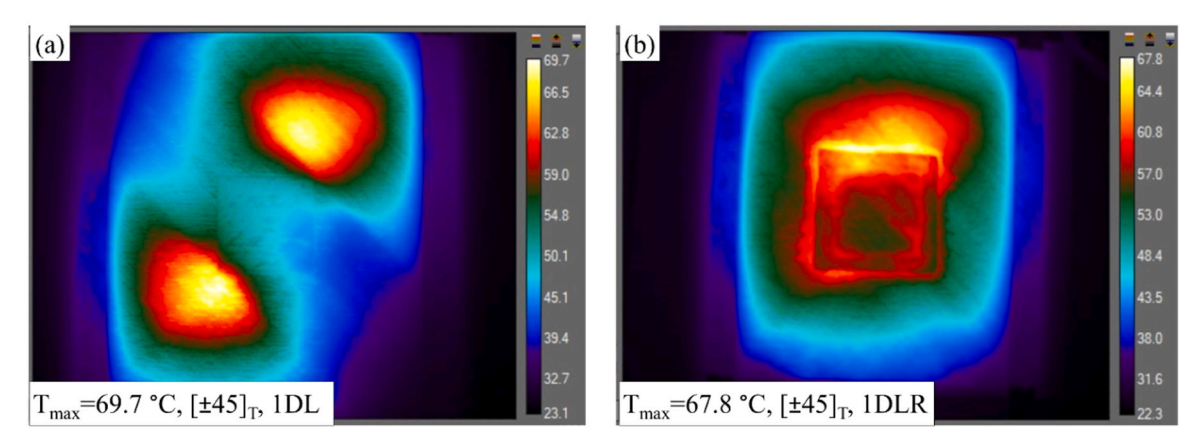


Fig. 23. Experimental results of thermal distribution and maximum temperature for  $[\pm 45]_T$  with one cutout layer and one layer intact at 2 V: a) damaged plate, b) plate after repair.

slight improvement compared to the damaged plate, but the resistance remains significantly higher, around a 27 % increase, when compared to the undamaged plate (see Table 7). In case of two cutout layers, the comparison between one-step (see Fig. 24-d) and two-step (see Fig. 24-c) repairs shows higher temperature for the repair in one step. As it appears, one-step repair results in better contact and thermal performance in the repaired area, which may be due to improved bonding between the layers compared to the two-step repair (this may be due to the two-step repair process, which results in a thicker resin layer within the patch region compared to the one-step repair). The electrical resistance of the plate shows that the one-step repair process resulted in a lower resistance (see Table 7), which is consistent with the thermal distribution. The resistance decreased by 37 % after repairing it in one-step (see Table 5), although it remains approximately 19 % higher than that of the original plate.

The results demonstrate that when multiple layers are damaged, it is more effective to repair all damaged layers in a single step rather than in multiple steps. Additionally, the plate with a 0° layer provides superior

performance compared to other configurations, both in terms of maximum temperature and thermal distribution.

### 2.7. Comparison between the experiment and numerical simulations

To illustrate the applied electric field in the FEM model, Fig. 25 shows representative contour plots of the electric potential distribution from electrode 1 to electrode 2. The numerical simulation results for laminates used in experiments are shown in this section (see Fig. 26). These results exhibit strong agreement with the experimental data (see Fig. 9), especially in terms of maximum temperature and thermal distribution. The deviation between the simulation and experimental results is about 4.5 %, which is within acceptable limits. For the damaged plate, the maximum difference between experimental values (see Fig. 19-a and Fig. 24-a) and numerical data (see Fig. 27-a and Fig. 27-b) is 5 %. Therefore, the model is considered validated and is suitable to simulate various types of damage and design optimal repair scenarios.

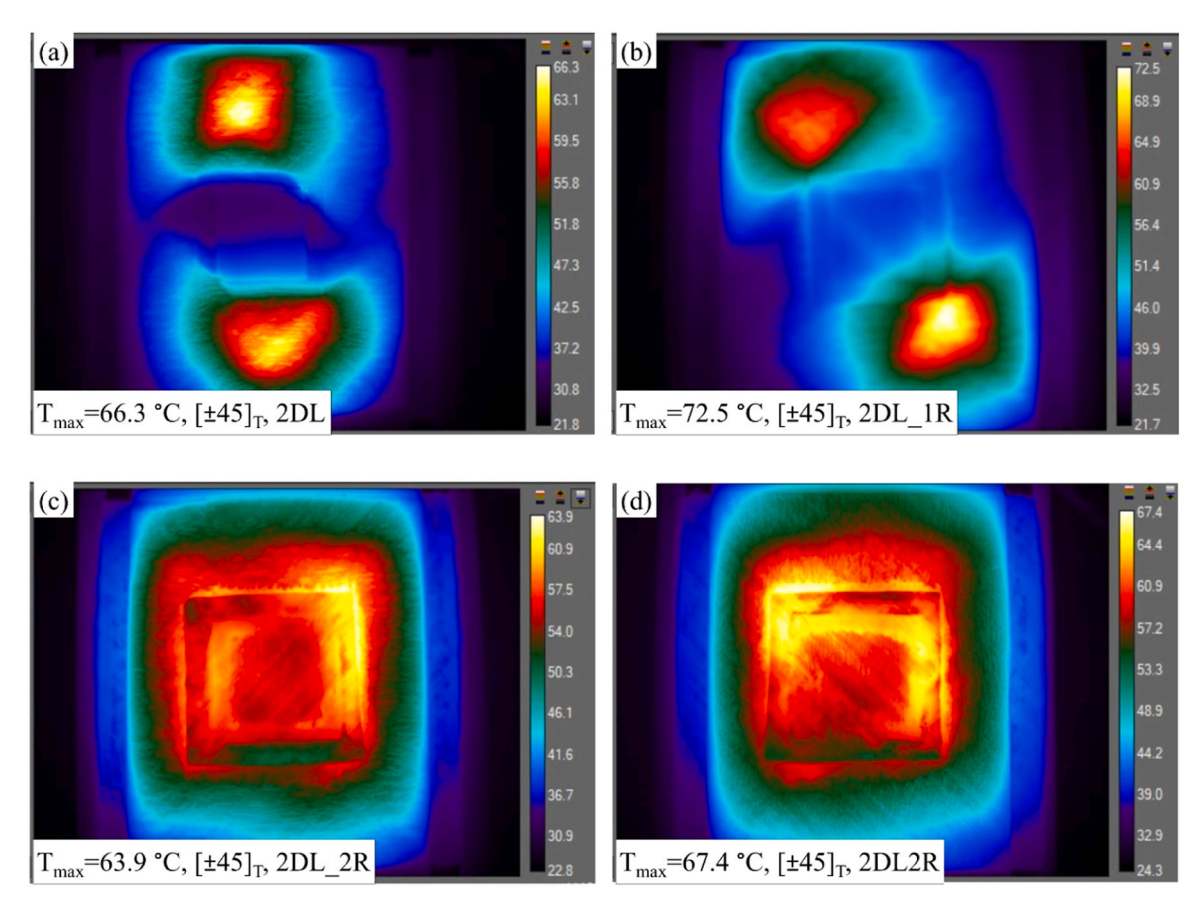


Fig. 24. Experimental results of thermal distribution and maximum temperature for  $[\pm 45]_T$  with two cutout layers (damage through the whole thickness) at 2 V: a) damaged plate, b) plate after repair only one layer, c) plate after repair two layers in two steps, d) plate after repair two layers in one step.

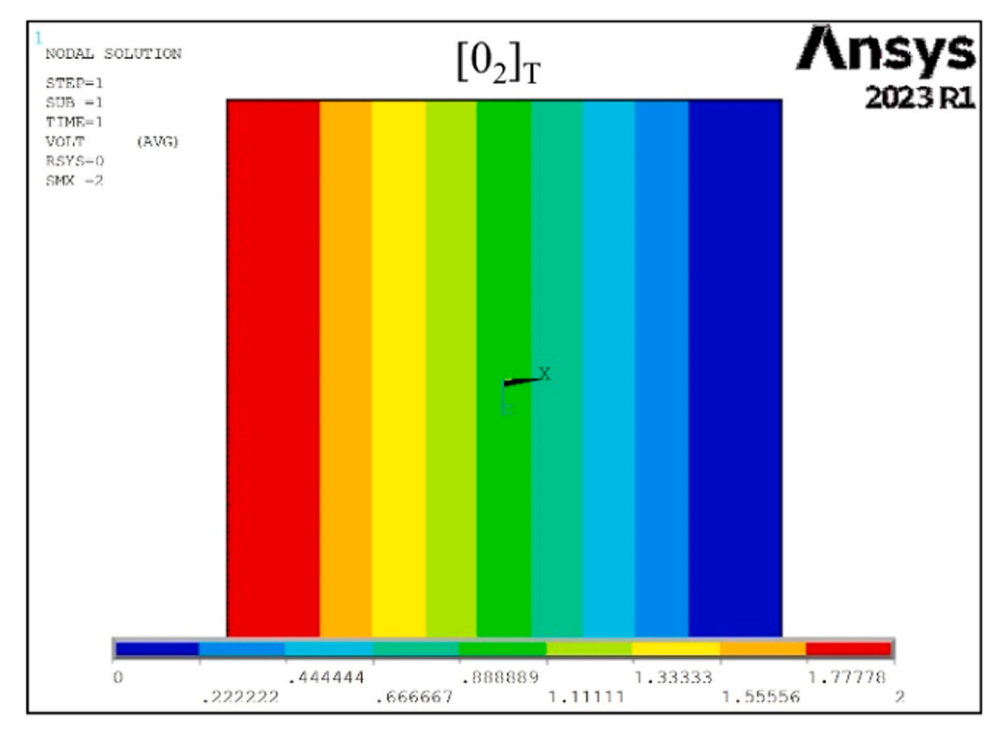


Fig. 25. Contour plots of electric potential distribution between electrode 1 and electrode 2 in the FEM model.

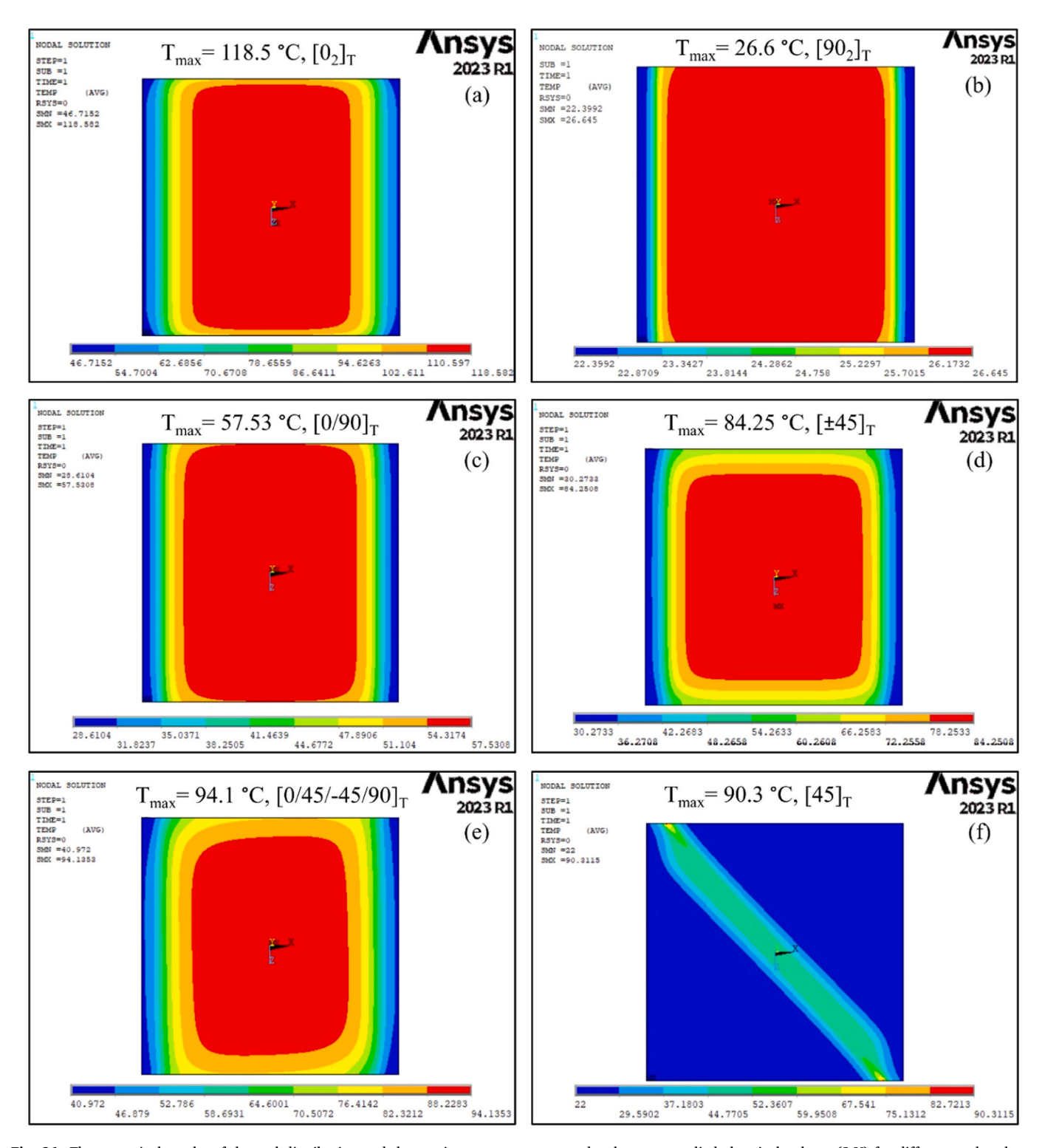
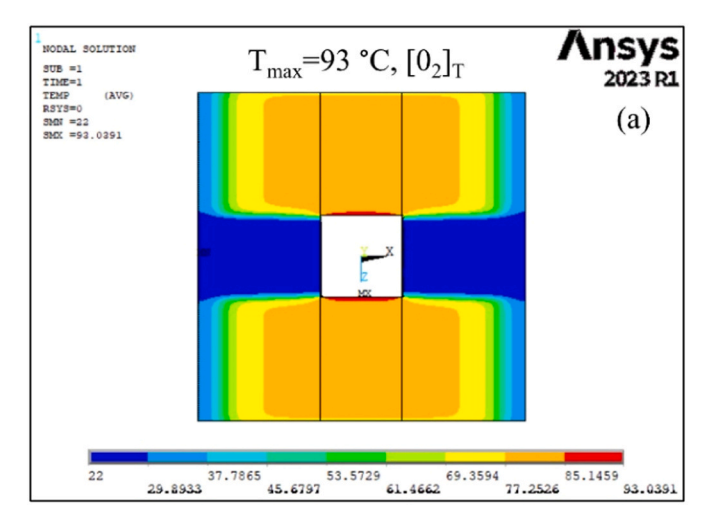


Fig. 26. The numerical results of thermal distribution and the maximum temperature under the same applied electrical voltage (2 V) for different carbon layer orientations: a)  $[0_2]_T$ , b)  $[90_2]_T$ , c)  $[0/90]_T$ , d)  $[\pm 45]_T$ , e)  $[0/45/-45/90]_T$ , f)  $[45]_T$  monoclinic materials.



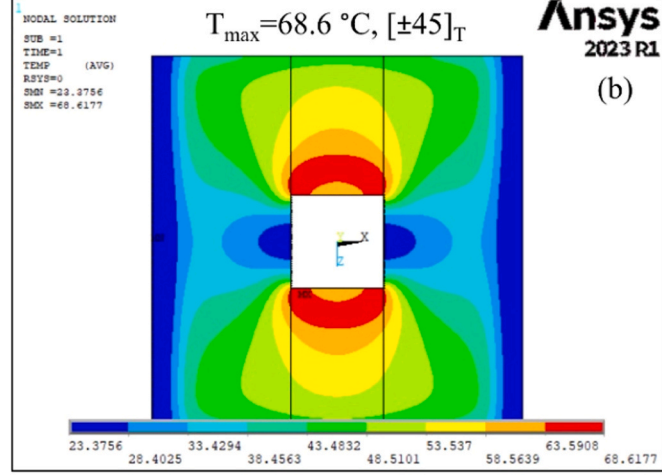


Fig. 27. The numerical results of thermal distribution and the maximum temperature under the same applied electrical voltage (2 V) for two different carbon layer orientations with two layers damaged: a)  $[0_2]_T$ , b)  $[\pm 45]_T$ .

#### 3. . Conclusions

This paper presents a comprehensive study of the electrical performance of carbon fiber laminates with different fiber orientations and under various conditions. The impact of damage on the resistance and heat generation in laminates is studied and different repair scenarios are considered. The experimental results are supported by the analytical calculations and numerical simulations. The numerical simulation results are closely aligned with the experimental findings, with a deviation of approximately 4.5 %, for undamaged plates while within 5 % for damaged plates confirming the model's accuracy. The developed numerical model is validated by the experimental data and can be used for design of composite laminates with tailored electrical properties. The simulations can be also employed to plan proper repair strategy for the conductive layer which generates heat.

Based on the obtained results for undamaged plates the following conclusions can be made:

- Fiber orientation significantly affects electrical resistance, unidirectional layup  $[0_2]_T$  has the lowest resistance, while cross-ply laminates  $[\pm 45]_T$ ,  $[0/90]_T$ , and  $[90_2]_T$  exhibit much higher resistance. The resistance is higher  $\approx 2$  and  $\approx 2000$  times than that of  $[0_2]_T$  compared to cross-ply and  $[90_2]_T$  laminates, respectively. The quasiisotropic laminates  $[0/45/-45/90]_T$  show twice as high resistance (after thickness normalization) compared to the 0-layer.
- Fiber orientation significantly affects temperature rise, different layer orientations lead to varying temperature increases under the same applied voltage (2 V). The  $[0_2]_T$  plate experiences the highest temperature rise due to its lower electrical resistance. The  $[0_2]_T$  plate's temperature was nearly twice that of the  $[0/90]_T$  plate, 40 % higher than the  $[45/-45]_T$  plate, and 4.5 times higher than the  $[90_2]_T$  plate. While the quasi-isotropic laminate  $[0/45/-45/90]_T$  shows a temperature rise only 25 % lower than  $[0_2]_T$ , likely due to increased fiber contact points through the thickness. This means that 0-layer is most efficient for heat generation.
- Inter-fiber interactions due to fiber misalignments and waviness enable some current flow even in the transverse direction. As well as the out-of-plane conductance and interaction between layers, which cannot be neglected for the theoretical calculation. However, it is not possible to predict the number of inter-fiber and/or inter-layer contacts as it strongly dependents on the method used to manufacture composite.

- The electrical resistance of laminates decreases with increasing temperature, but the change is not highly significant, indicating only a relatively small effect (3–6 %).

Considering the damage in laminates and the repair strategy the following statements can be made:

- The resistance changes in proportion to the reduction in effective conductive area (due to cutouts), with the most significant changes occurring in plates with  $\pm 45^{\circ}$  orientations.
- Increasing the plate length significantly raises resistance and reduces the maximum temperature in 0° fiber orientation plates due to the longer fibers. However, for other orientations (e.g. 45), inter-fiber contacts lead to a decrease in resistance and an increase in maximum temperature, primarily due to an increase in the effective conductive cross-sectional area.
- The repairing of multiple damaged layers in a single step yields better results than a multi-step approach, specifically in terms of thermal performance and electrical resistance.
- The 0° fiber orientation offers the best performance retention, making it the preferred choice for applications requiring high efficiency in electrical heating and thermal distribution.

While the present work focuses on laboratory-scale analysis, the findings provide a foundation for future studies on scalability, manufacturability, testing under actual conditions (frost, ice, and airflow), and the integration of the proposed repair strategies into full-scale structures such as wind turbine blades and aircraft components, where operational environments and long-term durability will require further consideration.

#### CRediT authorship contribution statement

Al-Ramahi Nawres Jabar: Writing – original draft, Methodology, Investigation, Data curation, Conceptualization. Patrik Fernberg: Writing – review & editing, Supervision, Project administration, Funding acquisition. Greger Nilsson: Validation, Methodology. Roberts Joffe: Writing – review & editing, Supervision, Resources, Project administration, Funding acquisition.

### **Declaration of Competing Interest**

The authors declare that they have no known competing financial interests or personal relationships that could have appeared to influence the work reported in this paper.

#### Acknowledgment

This project has received financial support from CREATERNITY at LTU.

The authors would like to acknowledge Nour Labidi for invaluable help with experiments. The authors also express gratitude to Birgitha Nyström from PODCOMP for providing the glass fiber sandwich panels.

#### Data availability

Data will be made available on request.

#### References

- [1] M. Kupke, K. Schulte, R. Schüler, Non-destructive testing of FRP by d.c. And a.c. Electrical methods, Compos. Sci. Technol. 61 (2001) 837–847, https://doi.org/ 10.1016/S0266-3538(00)00180-9
- [2] N. Athanasopoulos, V. Kostopoulos, Damage detection via joule effect for multidirectional carbon fiber reinforced composites, Appl. Phys. Lett. 101 (2012), https://doi.org/10.1063/1.4751992.
- [3] A. Galehdar, W.S.T. Rowe, K. Ghorbani, P.J. Callus, S. John, C.H. Wang, The effect of ply orientation on the performance of antennas in or on carbon fiber composites, Prog. Electromagn. Res. 116 (2011) 123–136, https://doi.org/10.2528/ PIER11031512.
- [4] M. Maria, Advanced composite materials of the future in aerospace industry, Incas Bull. 5 (2013) 139–150, https://doi.org/10.13111/2066-8201.2013.5.3.14.
- [5] T. Suzuki, J. Takahashi, LCA of lightweight vehicles by using CFRP for massproduced vehicles, Proc. 15th Int. Conf. Compos. Mater. (ICCM15) (2005) 1–4
- [6] G. Karalis, J. Zhao, M. May, M. Liebscher, I. Wollny, W. Dong, et al., Efficient joule heaters based on mineral-impregnated carbon-fiber reinforcing grids: an experimental and numerical study on a multifunctional concrete structure as an electrothermal device, Carbon N. Y. 222 (2024), https://doi.org/10.1016/j. carbon.2024.118898.
- [7] S. Siroka, B.M. Foley, M. Gralka, D. Fusco, S. Martis, The anisotropic electrical resistivity of a carbon fibre reinforced plastic disc and its use as a transducer, J. Phys. E 8 (5) (1975) 369–370.
- [8] K.W. Tse, C.A. Moyer, S. Arajs, Electrical conductivity of graphite fiber-epoxy resin composites, Mater. Sci. Eng. 49 (1981) 41–46, https://doi.org/10.1016/0025-5416 (81)90131-2
- [9] R.H. Knibbs, J.B. Morris, The effects of fibre orientation on the physical properties of composites, Composites 5 (1974) 209–218, https://doi.org/10.1016/0010-4361 (74)001414
- [10] D.R.P. Morris, J.T. Gostick, Determination of the in-plane components of the electrical conductivity tensor in PEM fuel cell gas diffusion layers, Electro Acta 85 (2012) 665–673, https://doi.org/10.1016/j.electacta.2012.08.083.
- [11] M. Weber, M.R. Kamal, Estimation of the volume resistivity of electrically conductive composites, Polym. Compos. 18 (6) (1997) 711–725, https://doi.org/ 10.1002/pc.10324.
- [12] N. Athanasopoulos, D. Sikoutris, T. Panidis, V. Kostopoulos, Numerical investigation and experimental verification of the joule heating effect of polyacrylonitrile-based carbon fiber tows under high vacuum conditions, J. Compos. Mater. 46 (18) (2012) 2153–2165, https://doi.org/10.1177/ 002198311430159
- [13] N. Athanasopoulos, V. Kostopoulos, Prediction and experimental validation of the electrical conductivity of dry carbon fiber unidirectional layers, Compos. B Eng. 42 (6) (2011) 1578–1587, https://doi.org/10.1016/j.compositesb.2011.04.008.
- [14] J.C. Abry, S. Bochard, A. Chateauminois, M. Salvia, G. Giraud, In situ detection of damage in CFRP laminates by electrical resistance measurements, Compos. Sci. Technol. 59 (1999) 925–935, https://doi.org/10.1016/S0266-3538(98)00132-8.
- [15] P.E. Irving, C. Thiagarajan, Fatigue damage characterization in carbon fibre composite materials using an electrical potential technique, Smart Mater. Struct. 7 (1998) 456–466, https://doi.org/10.1088/0964-1726/7/4/004.
- [16] A.S. Kaddour, F.A.R. Al-Salehi, S.T.S. Al-Hassani, M.J. Hinton, Electrical resistance measurement technique for detecting failure in CFRP materials at high strain rates, Compos. Sci. Technol. 51 (1994) 377–385, https://doi.org/10.1016/0266-3538 (94)90107-4.
- [17] J.B. Park, T. Okabe, N. Takeda, W.A. Curtin, Electromechanical modeling of unidirectional CFRP composites under tensile loading condition, Compos. Part A Appl. Sci. Manuf. 33 (2002) 267–275, https://doi.org/10.1016/S1359-835X(01) 00007-5
- [18] C.E. Bakis, A. Nanni, J.A. Terosky, S.W. Koehler, Self-monitoring, pseudo-ductile, hybrid FRP reinforcement rods for concrete applications, Compos. Sci. Technol. 61 (2001) 815–823, https://doi.org/10.1016/S0266-3538(00)00184-6.
- [19] N. Forintos, T. Czigany, Multifunctional application of carbon fiber reinforced polymer composites: electrical properties of the reinforcing carbon fibers – a short review, Compos. B Eng. 162 (2019) 331–343, https://doi.org/10.1016/j. compositesb.2018.10.098.
- [20] R. Prabhakaran, Damage assessment through electrical resistance measurement in graphite Fiber-Reinforced composites, Exp. Tech. 14 (1990) 16–20, https://doi. org/10.1111/j.1747-1567.1990.tb01059.x.

- [21] A. Todoroki, M. Tanaka, Y. Shimamura, High performance estimations of delamination of graphite/epoxy laminates with electric resistance change method, Compos. Sci. Technol. 63 (2003) 1911–1920, https://doi.org/10.1016/S0266-3538(03)00157.x
- [22] N. Angelidis, N. Khemiri, P.E. Irving, Damage detection in CFRP laminates using electrical potential techniques, Eur. Workshop Smart Struct. Eng. Technol. 4763 (2003) 156–162, https://doi.org/10.1117/12.508692.
- [23] A. Todoroki, The effect of number of electrodes and diagnostic tool for monitoring the delamination of CFRP laminates by changes in electrical resistance, Compos. Sci. Technol. 61 (2001) 1871–1880, https://doi.org/10.1016/S0266-3538(01) 00088.4
- [24] L. Hou, S.A. Hayes, A resistance-based damage location sensor for carbon-fibre composites, Smart Mater. Struct. 11 (2002) 966–969, https://doi.org/10.1088/ 0964-1726/11/6/401.
- [25] J.W. Cho, J.S. Choi, Relationship between electrical resistance and strain of carbon fibers upon loading, J. Appl. Polym. Sci. 77 (2000) 2082–2087, https://doi.org/ 10.1002/1097-4628(20000829)77:9<2082::AID-APP26>3.0.CO;2-W.
- [26] N. Angelidis, C.Y. Wei, P.E. Irving, The electrical resistance response of continuous carbon fibre composite laminates to mechanical strain, Compos. Part A Appl. Sci. Manuf. 35 (2004) 1135–1147, https://doi.org/10.1016/j. compositesa.2004.03.020.
- [27] S. Wang, D.D.L. Chung, Temperature/light sensing using carbon fiber polymer-matrix composite, Compos. B Eng. 30 (1999) 591–601, https://doi.org/10.1016/S1359-8368(99)00020-7.
- [28] C. Jeong, T.H. Lee, S.M. Noh, Y.Bin Park, Real-time in situ monitoring of manufacturing process and CFRP quality by relative resistance change measurement, Polym. Test. 85 (2020) 106416, https://doi.org/10.1016/j. polymertesting.2020.106416.
- [29] L. Selvakumaran, Q. Long, S. Prudhomme, G. Lubineau, On the detectability of transverse cracks in laminated composites using electrical potential change measurements, Compos. Struct. 121 (2015) 237–246, https://doi.org/10.1016/j. compstruct.2014.11.008.
- [30] N. Forintos, T. Czigany, Reinforcing carbon fibers as sensors: the effect of temperature and humidity, Compos. Part A Appl. Sci. Manuf. 131 (2020), https://doi.org/10.1016/j.compositesa.2020.105819.
- [31] D. Wang, D.D.L. Chung, Through-thickness piezoresistivity in a carbon fiber polymer-matrix structural composite for electrical-resistance-based throughthickness strain sensing, Carbon N. Y. 60 (2013) 129–138, https://doi.org/ 10.1016/j.carbon.2013.04.005.
- [32] S. Wang, D.D.L. Chung, Self-sensing of flexural strain and damage in carbon fiber polymer-matrix composite by electrical resistance measurement, Carbon N. Y. 44 (2006) 2739–2751. https://doi.org/10.1016/j.carbon.2006.03.034.
- [33] H.D. Roh, S.Y. Lee, E. Jo, H. Kim, W. Ji, Y.Bin Park, Deformation and interlaminar crack propagation sensing in carbon fiber composites using electrical resistance measurement, Compos. Struct. 216 (2019) 142–150, https://doi.org/10.1016/j. compstruct.2019.02.100.
- [34] A. Vavouliotis, A. Paipetis, V. Kostopoulos, On the fatigue life prediction of CFRP laminates using the electrical resistance change method, Compos. Sci. Technol. 71 (2011) 630–642, https://doi.org/10.1016/j.compscitech.2011.01.003.
- [35] T.J. Swait, F.R. Jones, S.A. Hayes, A practical structural health monitoring system for carbon fibre reinforced composite based on electrical resistance, Compos. Sci. Technol. 72 (2012) 1515–1523, https://doi.org/10.1016/j. compscitech.2012.05.022
- [36] D.J. Kwon, P.S. Shin, J.H. Kim, Z.J. Wang, K.L. DeVries, J.M. Park, Detection of damage in cylindrical parts of carbon fiber/epoxy composites using electrical resistance (ER) measurements, Compos. B Eng. 99 (2016) 528–532, https://doi. org/10.1016/j.compositesb.2016.06.050.
- [37] Q. Zhao, K. Zhang, S. Zhu, H. Xu, D. Cao, L. Zhao, et al., Review on the electrical resistance/conductivity of carbon fiber reinforced polymer, Appl. Sci. (Switz.) 9 (2019), https://doi.org/10.3390/app9112390.
- [38] A. Motaghi, A. Hrymak, G.H. Motlagh, Electrical conductivity and percolation threshold of hybrid carbon/polymer composites, J. Appl. Polym. Sci. 132 (2015) 1–9, https://doi.org/10.1002/app.41744.
- [39] Z. Liu, Y. Xu, X. Zhang, Y. Pei, Y. Cheng, W. Yin, Simulation study on the characteristics of carbon-fiber-reinforced plastics in electromagnetic tomography nondestructive evaluation systems, Int. Conf. Meas. Technol. Mechatron. Autom. ICMTMA 2010 20103 (2010) 382–385, https://doi.org/10.1109/ ICMTMA.2010.787.
- [40] X. Li, 2012, Eddy Current Techniques for Non-destructive Testing of Carbon Fibre Reinforced Plastic (CFRP). University of Manchester 2012:1–185.
- [41] R. Schueler, S.P. Joshi, K. Schulte, Damage detection in CFRP by electrical conductivity mapping, Compos. Sci. Technol. 61 (2001) 921–930, https://doi.org/ 10.1016/S0266-3538(00)00178-0.
- [42] M. Zappalorto, F. Panozzo, P.A. Carraro, M. Quaresimin, Electrical response of a laminate with a delamination: modelling and experiments, Compos. Sci. Technol. 143 (2017) 31–45, https://doi.org/10.1016/j.compscitech.2017.02.023.
- [43] Y.C. Shin, E. Novin, H. Kim, Electrical and thermal conductivities of carbon fiber composites with high concentrations of carbon nanotubes, Int. J. Precis. Eng. Manuf. 16 (2015) 465–470, https://doi.org/10.1007/s12541-015-0063-8.
- [44] R.B. HESLEHURSTStructural repair methodology for wind turbine blades. In: de ACS Australian Composites Conference, Gold Coast, Queensland.2015.
- [45] R.B. HESLEHURST, Analysis and modelling of damage and repair of composite materials in aerospace. Numerical Analysis and Modelling of Composite Materials, Springer Netherlands, Dordrecht, 1996, pp. 27–59.
- [46] D.J. Lekou, P. Vionis, Report on repair techniques for composite parts of wind turbine blades, Optimat Blades, 2002.

- [47] H.-C. LU, UV-cured adhesives for carbon fiber composite applications. Phd thesis, Purdue University (2013).
- [48] S. Halliwell, National composites network best practice guide: repair of fibre reinforced polymer (FRP) structures, National Composites Network, 2007.
- [49] Adhesive Joints and Patch Repair. Bureau Veritas, France. Guidance Notes NI 613 DT R00 E: 2015.
- [50] K. Bujun, 2014, Processing Study of in-situ Bonded Scarf Repairs for Composite Structures. Master Thesis. McGill University.
- [51] Y. Cui, W. Chen, N. Dai, C. Han, Integrated technologies for Anti-Deicing functions and structures of aircraft: current status and development trends, Aerospace 11 (2024), https://doi.org/10.3390/aerospace11100821.
- [52] H. Zhang, H. Guo, R. Jiang, W. Wan, P. Deng, X. Zhou, Research progress of multifunctional anti-icing composites materials, J. Appl. Polym. Sci. 141 (2024), https://doi.org/10.1002/app.55922.
- [53] H. Li, Q. Hu, X. Jiang, Z. Yu, L. Shu, C. Li, , 2022, Review on anti-icing and de-icing techniques of wind turbine blades.
- [54] Z. Zhao, X. Li, W. Li, M. Liu, Z. Hu, T. Jiang, et al., Progress in mechanism design of functional composites for anti-ice/deicing materials, Surf. Sci. Technol. 2 (2024), https://doi.org/10.1007/s44251-023-00033-2.
- [55] Torayca, 2015, T700S Data Sheet Carbon 2015:1-2.
- [56] K.C. Shin, J.J. Lee, Effects of thermal residual stresses on failure of co-cured lap joints with steel and carbon fiber-epoxy composite adherends under static and fatigue tensile loads, Compos Part A Appl. Sci. Manuf. 37 (2006) 476–487.
- [57] Mechanical properties of glass fiber reinforced polymer unidirectional lamina. These material properties from the website of Performance Composites Limited company. URL (\(\lambda\)http://www.performance-composites.com/carbonfibre/\(\rangle\) mechanical properties 2.asp\(\rangle\).